The Zonal Patterns in Late Quaternary Tropical South American Precipitation

T. Kukla[1,2] ![ORCID], **M. J. Winnick[3]** ![ORCID], **M. M. Laguë[4,5]** ![ORCID], **and Z. Xia[3,6]** ![ORCID]

[1]Department of Geosciences, Colorado State University, Fort Collins, CO, USA, [2]Department of Geological Sciences, Stanford University, Stanford, CA, USA, [3]Department of Earth, Geographic, and Climate Sciences, University of Massachusetts Amherst, Amherst, MA, USA, [4]University of Saskatchewan Coldwater Lab, Canmore, AB, Canada, [5]Department of Atmospheric Sciences, University of Utah, Salt Lake City, UT, USA, [6]Key Laboratory of Geogrpahical Processes and Ecological Security in Changbai Mountains, Ministry of Education, School of Geographical Sciences, Northeast Normal University, Changchun, China

Abstract Speleothem oxygen isotope records (δ^{18}O) of tropical South American rainfall in the late Quaternary show a zonal "South American Precipitation Dipole" (SAPD). The dipole is characterized by opposing east-west precipitation anomalies compared to the present—wetter in the east and drier in the west at the mid-Holocene ($\sim$7 ka), and drier in the east and wetter in the west at the Last Glacial Maximum ($\sim$21 ka). However, the SAPD remains enigmatic because it is expressed differently in western versus eastern δ^{18}O records and isotope-enabled climate model simulations usually misrepresent the magnitude and/or spatial pattern of δ^{18}O change. Here, we address the SAPD enigma in two parts. First, we re-interpret the δ^{18}O data to account for upwind rainout effects that are known to be pervasive in tropical South America, but are not always considered in Quaternary paleoclimate studies. Our revised interpretation reconciles the δ^{18}O data with cave infiltration and other proxy records, and indicates that the centroid of tropical South American rainfall has migrated zonally over time. Second, using an energy balance model of tropical atmospheric circulation, we hypothesize that zonal migration of the precipitation centroid can be explained by regional energy budget shifts, such as changing Saharan albedo associated with the African Humid Period, that have not been modeled in previous SAPD studies. This hypothesis of a migrating precipitation centroid presents a new framework for interpreting δ^{18}O records from tropical South America and may help explain the zonal rainfall anomalies that predate the late Quaternary.

Plain Language Summary Paleoclimate data suggest that, in the last $\sim$25,000 years, tropical South American precipitation has changed substantially, but in opposite directions between the east and west. This opposing east-west pattern in past rainfall is known as the "South American Precipitation Dipole," and its end-member states approximately coincide with the Last Glacial Maximum ($\sim$21,000 years ago) and mid-Holocene ($\sim$7,000 years ago), respectively. However, the cause of the dipole is debated because different models produce different results, and the interpretations of data are in conflict. Central in this conflict are oxygen isotope tracers of past precipitation which show different trends over space. We present a new interpretation of these data, backed by model results, which suggests that the dipole is driven by the centroid, or focus, of tropical South American precipitation migrating from west-to-east (and back) across tropical South America. We test this precipitation centroid migration hypothesis with an energy balance climate model which reproduces the expected east-west differences for the Last Glacial Maximum and mid-Holocene. The precipitation centroid migration hypothesis is a possible solution to the precipitation dipole enigma, but it remains to be tested in more sophisticated climate models.

1. Introduction

Tropical South America spans about one-tenth of the Earth's circumference from east to west (zonally). There is mounting evidence that rainfall across this stretch has varied in a zonal "dipole" fashion in the late Quaternary (here, the last $\sim$25 kyr) with rainfall increasing in northeastern Brazil at the expense of drying in western Amazonia, and vice versa (M. C. Campos et al., 2022; Cheng et al., 2013; Cruz et al., 2009; Martin et al., 1997). This zonal rainfall pattern is called the "South American Precipitation Dipole" (SAPD), a term that describes the opposing east-west patterns of past rainfall anomalies (Figures 1a and 1b), and is distinct from the precipitation dipole studied in the modern climate between southeastern South America and the South Atlantic
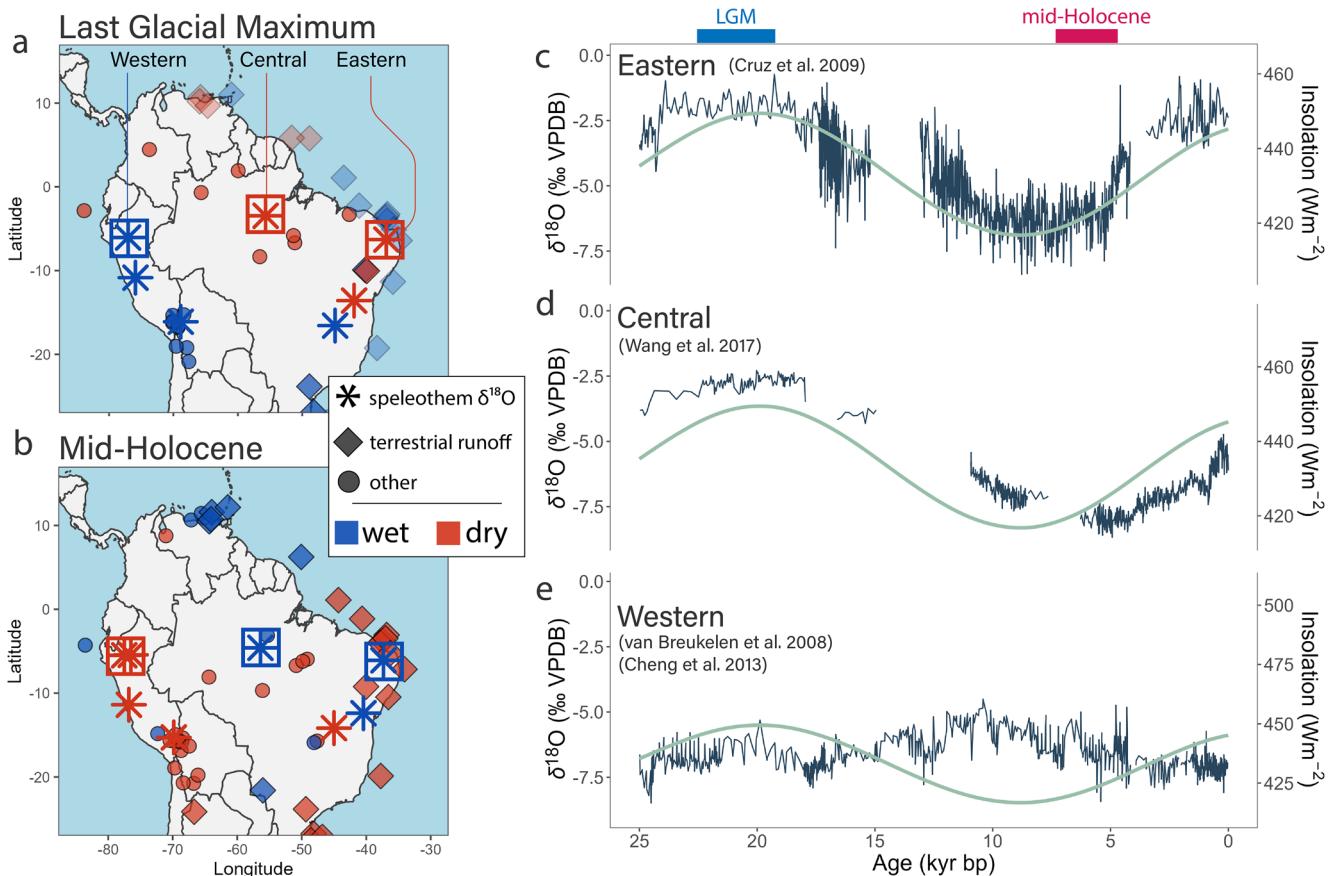
Figure 1. *South America proxy map and isotope data*. Proxy map for the (a) Last Glacial Maximum (LGM) (∼21) and (b) mid-Holocene (∼7 ka). Data points in panels (a, b) are jittered to show instances of multiple proxy records from the same site. Offshore runoff proxies are lighter in panel (a) because they can record a sea-level signal at the LGM. (c) Rio Grande do Norte (eastern) δ¹⁸O record (Cruz et al., 2009). (d) Paraíso (central) δ¹⁸O record (Wang et al., 2017). (e) Diamante and Tigre Perdido composite (western) δ¹⁸O record (Cheng et al., 2013; van Breukelen et al., 2008). Teal lines (c–e) show February insolation at 10°S following Cruz et al. (2009) (scales varied to match δ¹⁸O magnitude).

Convergence Zone (Boers et al., 2014; Nogués-Paegle & Mo, 1997). The SAPD has been identified on precession (Cheng et al., 2013; Cruz et al., 2009; Martin et al., 1997; Wang et al., 2004) and glacial-interglacial timescales (Abouchami & Zabel, 2003; Mason et al., 2019), and it corresponds with many high-amplitude signals in paleoclimate proxy data (P. A. Baker, Rigsby, et al., 2001; P. A. Baker, Seltzer, et al., 2001; Cruz et al., 2009; Fritz et al., 2004; Tapia et al., 2003; Wang et al., 2017). Still, conflicting model and proxy interpretations cast doubt on what drives the SAPD (M. C. Campos et al., 2022; Cruz et al., 2009; Liu & Battisti, 2015), and even whether it exists at all (Wang et al., 2017).

On precession timescales, a primary challenge of the SAPD enigma is how to interpret the speleothem oxygen isotope (δ¹⁸O) records that span the dipole region (Figures 1c–1e). These spatially and temporally complex δ¹⁸O records are difficult to reconcile with some independent proxy data. From the relatively high austral summer insolation phase around the Last Glacial Maximum (LGM, ∼21 ka) to the lower phase at the mid-Holocene (∼7 ka), the speleothem δ¹⁸O records are zonally imbalanced—the δ¹⁸O shifts to the east are about twice as large as the opposing shifts in the west. East δ¹⁸O is, if anything, less sensitive to precipitation amount than west δ¹⁸O today (Figure S1 in Supporting Information S1), so it is speculated that these data imply a zonally imbalanced SAPD with larger precipitation anomalies in the east (Cheng et al., 2013). Yet, the implication of a more quiescent precipitation history in the west is not consistent with previous evidence for substantial drying from the wetter-than-present LGM to the mid-Holocene (P. A. Baker, Rigsby, et al., 2001; P. A. Baker, Seltzer, et al., 2001; Fritz et al., 2004; Tapia et al., 2003). Further, evidence from strontium isotopes in speleothems across tropical South America shows δ¹⁸O is often decoupled from rainfall amount (Ward et al., 2019; Wortham et al., 2017). Thus, it is not clear that zonally imbalanced δ¹⁸O signals require a zonally imbalanced SAPD.

The speleothem $\delta^{18}O$ data also reveal important discrepancies with isotope-enabled General Circulation Models (GCMs) forced with precession. In isotope-enabled GCMs, opposing east-west precipitation and $\delta^{18}O$ anomalies have a similar magnitude—the SAPD is zonally balanced (Cruz et al., 2009; Liu & Battisti, 2015). Under low summer insolation, precipitation $\delta^{18}O$ decreases by 1‰–3‰ in the east, increases by the same amount in the west, and shows no change in east-central Amazonia where there is a large ~6‰ shift in the speleothem data (Cruz et al., 2009; Liu & Battisti, 2015; Wang et al., 2017). Thus, while the direction of change is reasonable, the magnitude and spatial pattern of $\delta^{18}O$ is inconsistent with the speleothem data, suggesting factors other than precession may contribute to the late Quaternary SAPD. Precession may also be insufficient to explain the apparent out-of-phase changes in speleothem $\delta^{18}O$ in the last ~15 kyr (Figures 1c–1e). Precession-driven insolation forcing is uniform east-to-west, but minimum and maximum $\delta^{18}O$ values occur at different times across tropical South America.

The goal of this manuscript is to develop a conceptual model for the late Quaternary SAPD that is consistent with the enigmatic features of the oxygen isotope records—namely the zonally imbalanced $\delta^{18}O$ signals and their out-of-phase nature. We begin by reinterpreting the $\delta^{18}O$ data to account for the effect of upwind rainout (where upwind is east). Upwind rainout can decouple local $\delta^{18}O$ from local rainfall amount by generating low-$\delta^{18}O$ moisture that is transported downwind. The effect is widely known to drive Amazon $\delta^{18}O$ in modeling, observational, and paleoclimate studies (Ampuero et al., 2020; J. C. A. Baker et al., 2016; Brienen et al., 2012; Gat & Matsui, 1991; Grootes et al., 1989; Salati et al., 1979; Vimeux et al., 2005; Vuille & Werner, 2005; Vuille et al., 2003), yet has not been empirically constrained in previous interpretations of the SAPD (Cheng et al., 2013; Cruz et al., 2009; van Breukelen et al., 2008). Accounting for upwind rainout yields two important results. First, it brings the $\delta^{18}O$ data in better agreement with other proxy records, including strontium isotopes, and casts the SAPD as zonally balanced—the magnitude of precipitation anomalies is similar in the east and west. Second, the $\delta^{18}O$ data can be understood as recording zonal shifts in the location of maximum rainout, or the "precipitation centroid," across tropical South America. A precipitation centroid that migrates east-west reconciles a zonally balanced SAPD with zonally imbalanced $\delta^{18}O$ anomalies and it explains the out-of-phase $\delta^{18}O$ signals. Yet, the mechanisms for a zonally migrating precipitation centroid are not immediately clear.

In the second part of our analysis, we test whether precession forcing can explain a migrating precipitation centroid. Precession is considered the primary driver of the SAPD, and it was previously linked to east-west shifts in the pan-Asian Monsoon precipitation centroid (Battisti et al., 2014). These zonal pan-Asian Monsoon shifts caused large changes in $\delta^{18}O$ and precipitation, and we find similarly large changes in South America using an isotope-enabled reactive transport model (Kukla et al., 2019). However, the same GCM simulations presented in Battisti et al. (2014) showed no zonal migration in the tropical South American precipitation centroid, and we also find no zonal shifts in the PMIP3/CMIP5 models. Instead, we posit that land surface albedo change, in addition to precession, can explain the late Quaternary SAPD. We impose reasonable late Quaternary land albedo forcings in an energy balance model for tropical atmospheric circulation and find zonal shifts in the South American precipitation centroid that are consistent with the isotope data. We conclude that, while precession can drive a zonal precipitation dipole, additional forcings such as land albedo are necessary to explain the zonal imbalance of $\delta^{18}O$ signals, their magnitude, and their out-of-phase trends.

2. Late Quaternary Speleothem $\delta^{18}O$ Records and Precipitation Dynamics

Our analysis leverages three existing speleothem $\delta^{18}O$ records that span tropical South America and have previously been used to identify the SAPD. We refer to these as the eastern, central, and western records (Figure 1). The eastern record is from the Rio Grande do Norte site of northeastern Brazil and shows a 5‰–7‰ decrease in $\delta^{18}O$ from the LGM to early mid Holocene interpreted as evidence for a weakening South American Monsoon (Cruz et al., 2009) (Figure 1c). The central record comes from the Paraíso site in east-central Amazonia (Wang et al., 2017) and resembles the eastern record, but the $\delta^{18}O$ decrease lags behind by 1–2 kyr, and the records diverge in the late Holocene (Figure 1d). Given its location near the monsoon's deep convective region, data from the central site were interpreted as evidence for stronger convection in the mid-Holocene, in conflict with the eastern record interpretation (Wang et al., 2017). The western record is a composite of the Diamante (Cheng et al., 2013) and Tigre Perdido (van Breukelen et al., 2008) records (Figure 1e). We adopt the cave temperature correction for these records following Wang et al. (2017) (see also Ampuero et al. (2020) and Kukla et al. (2021)), increasing $\delta^{18}O$ by 1.4‰ to account for its relatively cooler cave temperatures. These records are interpreted to

reflect Amazon or western Amazon rainfall amount, with a muted $\delta^{18}O$ increase of ∼2.5‰ from the LGM to early Holocene indicative of drying, then a gradual decrease to wetter, present conditions that starts when the eastern and then central $\delta^{18}O$ records initially decrease. The western record stands out from the central and eastern records in that $\delta^{18}O$ increases, rather than decreases, from the LGM to the early mid Holocene. This contrast defines the $\delta^{18}O$ expression of the SAPD, with the western-wet phase at the LGM and eastern-wet phase at the mid-Holocene representing end-member SAPD states.

The zonal SAPD is likely driven by multiple factors but, on precession timescales, it is agreed that changes in austral summer insolation are critical (M. C. Campos et al., 2022; Cheng et al., 2013; Cruz et al., 2009; Liu & Battisti, 2015; Prado et al., 2013). Precession drives summer insolation with a ∼21 kyr beat, and this forcing carries no zonal component. Low austral summer insolation (as during the mid-Holocene, ∼7 ka) weakens the South American Monsoon and decreases rainfall in western tropical South America (P. A. Baker, Seltzer, et al., 2001; M. C. Campos et al., 2022; Cruz et al., 2009; Liu & Battisti, 2015). However, the opposing increase in eastern precipitation requires some zonal shift in atmospheric circulation, and the cause is debated. One theory posits that weaker subsidence over northeast Brazil must compensate for weaker convection to the west, increasing northeast Brazil rainfall (M. C. Campos et al., 2022; Cruz et al., 2009; Shimizu et al., 2020). Another argues that northeast Brazil rainfall increases as south African summer cooling shifts the subtropical rain band, the South Atlantic Convergence Zone, northward, and north African cooling shifts the tropical rain band, the Inter-Tropical Convergence Zone (ITCZ), southward (Liu & Battisti, 2015), consistent with a broader seasonal ITCZ migration (Chiessi et al., 2021). In both cases models capture zonally opposing $\delta^{18}O$ anomalies, but not their zonal imbalance, nor the magnitude of eastern and central $\delta^{18}O$ change (note that the central record was published after Cruz et al. (2009) and Liu and Battisti (2015)). Moreover, other simulations with precession forcing find no SAPD, or a zonal precipitation dipole in the austral summer that is offset by opposing anomalies in the austral winter (Prado et al., 2013; Shimizu et al., 2020; Tigchelaar & Timmermann, 2016). One key limitation in the application of these models to the mid-Holocene is they do not account for the greening-induced decrease in Saharan land albedo—a major boundary condition change that has previously been linked to rainfall anomalies in tropical South America (Lu et al., 2021). If such zonal forcings can impact tropical South American rainfall, they may be critical for explaining the zonal patterns of the SAPD.

Recent theoretical work demonstrates that South American rainfall, more so than other tropical regions, is energetically primed to shift east-west due to factors like non-local land surface albedo change (Boos & Korty, 2016). The precipitation centroid in tropical South America sits at the intersection of the energy flux equator (EFE) (correlated with the ITCZ) and an energy flux prime meridian (EFPM) (Boos & Korty, 2016). These energy flux lines occur where column-integrated divergent atmospheric energy transport is zero in the meridional (EFE) and zonal (EFPM) directions (Boos & Korty, 2016). The EFE-prime meridian intersection conditions the precipitation centroid to migrate zonally because, just as the EFE (and ITCZ) moves north and south following anomalous meridional energy sources (e.g., changes in insolation and albedo), the EFPM moves west and east in response to zonal energy anomalies. North-south shifts in the precipitation centroid, following the EFE, are well documented in tropical South America and elsewhere (Arbuszewski et al., 2013; J. L. P. S. Campos et al., 2019; Chiessi et al., 2021; Deplazes et al., 2013; Haug, 2001; Mulitza et al., 2017), but east-west shifts are less thoroughly explored. The pan-Asian monsoon is also associated with an EFPM and has been shown to migrate zonally with high-amplitude precession forcing, though precession alone appears insufficient to shift the precipitation centroid east-west in South America (Battisti et al., 2014; Liu & Battisti, 2015; Shimizu et al., 2020). If other factors drove the EFPM over South America to shift zonally in the past, we expect the precipitation centroid to shift with it (Boos & Korty, 2016), driving a zonal dipole in rainout expressed as the SAPD.

3. Methods

3.1. Paleo-Isotope Gradient Justification

The isotope gradient is defined as downwind $\delta^{18}O$ minus upwind $\delta^{18}O$ along a given moisture trajectory and it is expressed in units of ‰ per thousand kilometers. This change in $\delta^{18}O$ is related to Rayleigh distillation interpretations of isotopic data as both $\delta^{18}O$ and $\Delta\delta^{18}O$ decrease as net rainout (or distillation) increases (Gat & Matsui, 1991; Salati et al., 1979). Whereas one must assume the upwind $\delta^{18}O$ value to interpret a given $\delta^{18}O$ record in terms of net rainout, $\Delta\delta^{18}O$ explicitly accounts for these upwind variations, theoretically isolating the $\delta^{18}O$ signal due to rainout alone (Hu et al., 2008; Kukla et al., 2019, 2021; Winnick et al., 2014). This approach
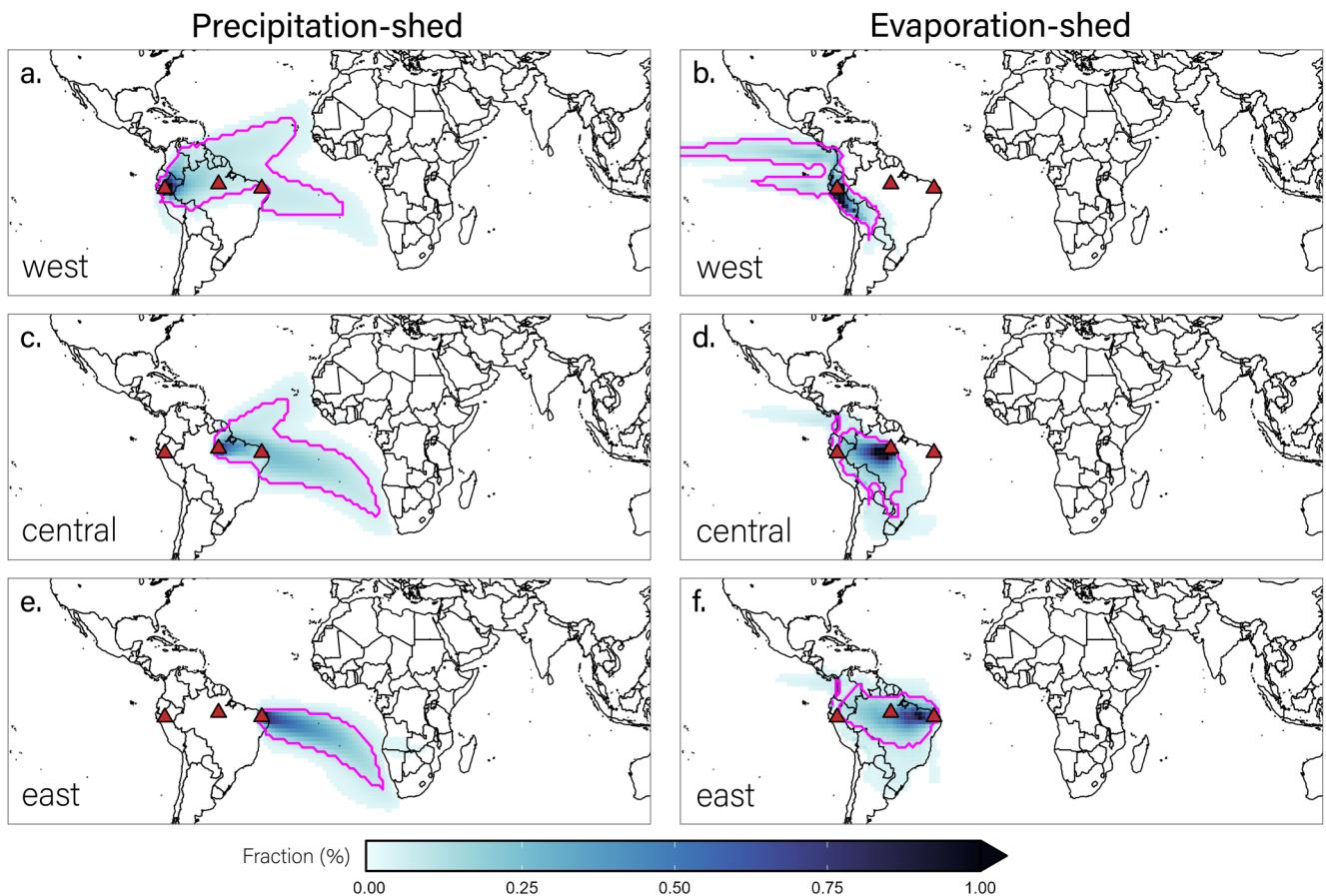
Figure 2. *WAM-2layers hydrologic connectivity between speleothem sites.* (a, c, and e) Annual mean precipitation-sheds and (b, d, and f) evaporation-sheds for the (a, b) western, (c, d) central, and (e, f) eastern sites. Magenta line denotes the spatial threshold where 70% of precipitation is sourced (precipitation-sheds) or where evaporation re-precipitates (evaporation-sheds), used to indicate a dynamically significant connection (Keys et al., 2012). Results show sites are significantly hydrologically connected within a single evaporation-precipitation cycle (See Supporting Information S1 for seasonal results).

is particularly useful in tropical South America because upwind effects are known to be a primary driver of $\delta^{18}O$ (Ampuero et al., 2020; J. C. A. Baker et al., 2016; Gat & Matsui, 1991; Lee et al., 2009; Liu & Battisti, 2015; Salati et al., 1979; Vuille & Werner, 2005; Vuille et al., 2003). Upwind and local rainout can be distinguished because upwind rainout will change the initial $\delta^{18}O$ of a given domain but not $\Delta\delta^{18}O$ (Kukla et al., 2021; Salati et al., 1979). We note that $\Delta\delta^{18}O$ values are generally restricted to below zero (the "hydrostat"), since a zero isotope gradient reflects all precipitation being recycled between two sites or zero or negligible precipitation (i.e., no net rainout) (Caves et al., 2015; Chamberlain et al., 2014; Kukla et al., 2019).

To validate our use of the isotope gradient approach, we analyze the connectivity of atmospheric moisture through transport and recycling among the eastern, central, and western sites in the modern climate. We use the 2-layer Water Accounting Model (WAM-2layers) (van der Ent et al., 2014) and the precipitation back-tracking scheme of Keys et al. (2012) (van der Ent, 2016; van der Ent & Savenije, 2013). The model simulates precipitation-sheds, the area where evaporation sources a site's precipitation, and evaporation-sheds, the area where a site's evaporation re-precipitates out. Contours enclosing the area where 70% of a site's rainfall is sourced (for precipitation-sheds) or a site's evaporation rains out (for evaporation-sheds) can be used to infer a meaningful dynamic connection between sites (Keys et al., 2012). We find that moisture recycling between our sites surpasses this threshold (Figure 2), demonstrating that these sites are sufficiently isotopically connected for $\Delta\delta^{18}O$ analysis (see Text S1, Figures S2 and S3 in Supporting Information S1). We also find that the modern isotope gradient across tropical South America is negatively correlated with rainout and is negative throughout the year, consistent with theory for upwind signals propagating downwind with minimal attenuation (Figure S4 in Supporting Information S1) (Kukla et al., 2019). Constraining the isotopic connectivity between sites is

challenging, in part because a strong connection today does not necessarily imply a strong connection in the past. Yet, as air-masses shift in response to past forcings, moisture at one site can still be recycled to the next. Today, moisture recycling connects regions across tropical South America that receive their peak rainfall at different times of the year (Staal et al., 2018). We discuss how weak isotopic connections would affect our conclusions in Section 5.4.

3.2. Reconstructing Paleo-Precipitation Rates From the Central-To-Western Sites

We focus exclusively on the isotope gradient between the central and western sites for our quantitative precipitation reconstruction because this trajectory aligns best with that of the prevailing winds (see Text S1 and S2 in Supporting Information S1). Oxygen isotope gradients along a dominant moisture trajectory depend on the balance of three fluxes: precipitation, evapotranspiration, and atmospheric transport (Salati et al., 1979; Winnick et al., 2014). We use a reactive transport model that simulates $\Delta\delta^{18}O$ as a function of these fluxes to quantify past precipitation rates from $\Delta\delta^{18}O$ data. To do so, we randomly sample from uniform distributions of reactive transport model input parameters to estimate past precipitation from the simulations that agree with $\Delta\delta^{18}O$ data (Kukla et al., 2019, 2021).

Our application of the reactive transport model to the central-to-western isotope gradient follows that of Kukla et al. (2021) with one key change. Kukla et al. (2021) used modern reanalysis data to analyze both the late Holocene and mid-Holocene isotope gradients because PMIP3/CMIP5 results (Braconnot et al., 2012) show that reactive transport model inputs are similar for both time periods. However, modern reanalysis data cannot be reasonably applied to the LGM due to the ~5°C of tropical cooling. To account for this cooling, we apply temperature-based scaling relationships to the reanalysis data to estimate LGM moisture content over the ocean (moisture source region) and potential evapotranspiration. Source region moisture content is calculated assuming relative humidity remains constant over the ocean (Sherwood et al., 2010), and potential evapotranspiration is decreased following the scaling relationship defined by Scheff and Frierson (2014) and Siler et al. (2019). Decreasing source moisture content and potential evapotranspiration both increase net rainout, all else equal. Therefore, these changes decrease the reconstructed LGM precipitation rates required to reproduce a given isotope gradient. Moisture content and humidity are allowed to change over land depending on model-simulated rainout. We further account for unique LGM conditions by restricting the wind speed and transpiration fraction estimates. Proxy studies (Bradtmiller et al., 2016; McIntyre & Molfino, 1996; Venancio et al., 2018) suggest that the northeasterlies were stronger at the LGM, so we restrict wind speeds to be equal to or greater than the late Holocene. Lower atmospheric $p\mathrm{CO}_2$ implies lower plant water use efficiency suggesting that more transpiration may have been necessary to fix (approximately) the same amount of carbon. Since the rainforest largely remained intact at the LGM (i.e., similar biomass), we assume the transpired fraction of evapotranspiration is also equal to or greater than modern.

We find that our results are not sensitive to the shape of the distributions of model inputs, nor the sample size of the Monte Carlo routine (Figure S5 in Supporting Information S1). We also test the importance of an additional input, rain re-evaporation, on model $\delta^{18}O$. Rain re-evaporation and its effect on $\delta^{18}O$ is heavily parameterized in models because it is difficult to directly measure (Dee et al., 2015; Konecky et al., 2019; Worden et al., 2007) (see Text S2 and S3 in Supporting Information S1). Using a parameterization fit to isotope data we find that it has a negligible effect on $\delta^{18}O$ in the model (Figure S6 in Supporting Information S1). Diagnostics of our late Holocene Monte Carlo results (essentially a modern analysis because late Holocene speleothem $\delta^{18}O$ is the same as modern rainfall) are provided in Figure S7 in Supporting Information S1.

We further use the reactive transport model to calculate spatial $\delta^{18}O$ patterns for individual PMIP3/CMIP5 models (Braconnot et al., 2012). Using zonal profiles of atmospheric moisture content, zonal winds, potential evapotranspiration, and temperature from the individual PMIP3/CMIP5 models, we run the reactive transport model to simulate the isotope gradient for the LGM, mid-Holocene, and late Holocene (PMIP3/CMIP5 pre-industrial). We then compare the predicted $\Delta\delta^{18}O$ derived from the PMIP3/CMIP5 data to the speleothem data. If the predicted $\Delta\delta^{18}O$ is more negative than the observed $\Delta\delta^{18}O$, then the net rainout in that model is too high to reconcile the observed data in the reactive transport framework. We also analyze the precipitation rate necessary to match the paleo-isotope gradient if all other PMIP3/CMIP5 inputs to the reactive transport model are correct. This analysis effectively asks how much rainfall must increase or decrease relative to the PMIP3/CMIP5 prediction in order to reconcile the paleoclimate $\Delta\delta^{18}O$ data.

3.3. Application of a 2-Dimensional Atmosphere Energy Balance Model

We use a 2-dimensional energy balance model that is capable of tracking zonal shifts in the precipitation centroid (Boos & Korty, 2016) to accomplish two related goals. First, we identify the precipitation centroid to test whether it shifts zonally in the mid-Holocene or LGM simulations of the PMIP3/CMIP5 models. Second, we simulate the zonal precipitation centroid response to conditions that likely characterize the LGM and mid-Holocene but are not accounted for in the PMIP3/CMIP5 experiments.

The energy balance model predicts how changes in energy input to the atmosphere would change atmospheric energy transport, thus altering atmospheric circulation and precipitation patterns. Here, we follow the methodology of Boos and Korty (2016) and consider how changes in continental albedo alter energy input to the atmosphere, and how atmospheric circulation would have to adjust in order to maintain the energy balance. The anomalous energy flux generated by the energy balance model is then used to infer a shift in precipitation based on the assumption that the position of peak precipitation migrates with the intersection of the EFE and EFPM (see Equations 2–7 in Boos and Korty (2016)). We refrain from attributing the precipitation centroid anomalies to a specific atmospheric feature because the model is not designed to distinguish between the individual effects of, for example, the South American Monsoon, the South Atlantic Convergence Zone, and the ITCZ.

3.3.1. Analysis of PMIP3/CMIP5 Precipitation Dynamics

Using the energy balance model, we identify the PMIP3/CMIP5 ensemble mean location of the precipitation centroid, defined as the intersection of the EFE and prime meridian, for the LGM, mid-Holocene, and pre-industrial (or late Holocene). The LGM and mid-Holocene ensemble means are then used as the initial conditions for the perturbations discussed in the next section.

3.3.2. Simulating Additional LGM and Mid-Holocene Constraints

A critical step in determining whether the precipitation centroid migrated zonally in the past is quantifying the sensitivity of zonal shifts to energetic forcing. We impose anomalous moist static energy (MSE) sources in the PMIP3/CMIP5 ensemble mean to quantify how the zonal location of the EFPM (and thus the precipitation centroid (Boos & Korty, 2016)) changes with zonal forcing. The response of the South American precipitation centroid to anomalous energy forcing depends on (a) the magnitude and direction of energetic forcing, (b) the area over which the forcing is applied, and (c) the distance (especially zonally) of the anomalous forcing to the centroid.

During the mid-Holocene, lower land surface albedo likely increased the net column energy over the grassy "green" Sahara by about 70 W/m^2, accounting for the attenuation of the albedo anomaly at the top of the atmosphere (Boos & Korty, 2016). This forcing exceeds the magnitude of insolation change due to orbital variability (~10 W/m^2 in the mid-Holocene), but is applied over a smaller area (confined to the modern Sahara). Other modeling investigations of the late Quaternary SAPD (including PMIP3/CMIP5 simulations) accounted for orbital forcing, but did not consider the Green Sahara (Cruz et al., 2009; Liu & Battisti, 2015). During the LGM there is evidence for forest dieback and grassland expansion in the African tropics, plus tundra expansion in the forests of modern Eurasia (Binney et al., 2017; Prentice et al., 2011; Wu et al., 2007). These vegetation shifts would have brightened the regional land surface and, barring strong compensating feedbacks, the top of atmosphere. We note that our analysis does not account for other factors outside of MSE anomalies that can shift the precipitation centroid zonally. For example, there is evidence for stronger easterly winds across the tropical Atlantic at the LGM (Adkins et al., 2006; Bradtmiller et al., 2016; McGee et al., 2013; McIntyre & Molfino, 1996; Zular et al., 2019) that could shift the maximum vector wind divergence, and thus precipitation centroid, westward, but stronger winds cannot be readily integrated to the energy balance model as an anomalous energy source.

Starting from the ensemble mean mid-Holocene and LGM climates, we simulate the effect of a darker Sahara (mid-Holocene) and a brighter African tropics and Eurasia (LGM) as spatially uniform positive and negative MSE anomalies, respectively. This approach carries some important limitations and should be taken as a proof of concept for demonstrating how land surface albedo can modulate the zonal location of the South American precipitation centroid. Our analysis implicitly assumes that the attenuation of the land surface anomaly to the top of atmosphere is spatially uniform, which is unlikely when comparing tropical Africa and Eurasia. This analysis also ignores the role of an apparent shift to a less El Niño-dominant mean climate state after the LGM (Ford et al., 2018; Koutavas & Joanides, 2012), which could affect the zonal energy balance (Boos & Korty, 2016)
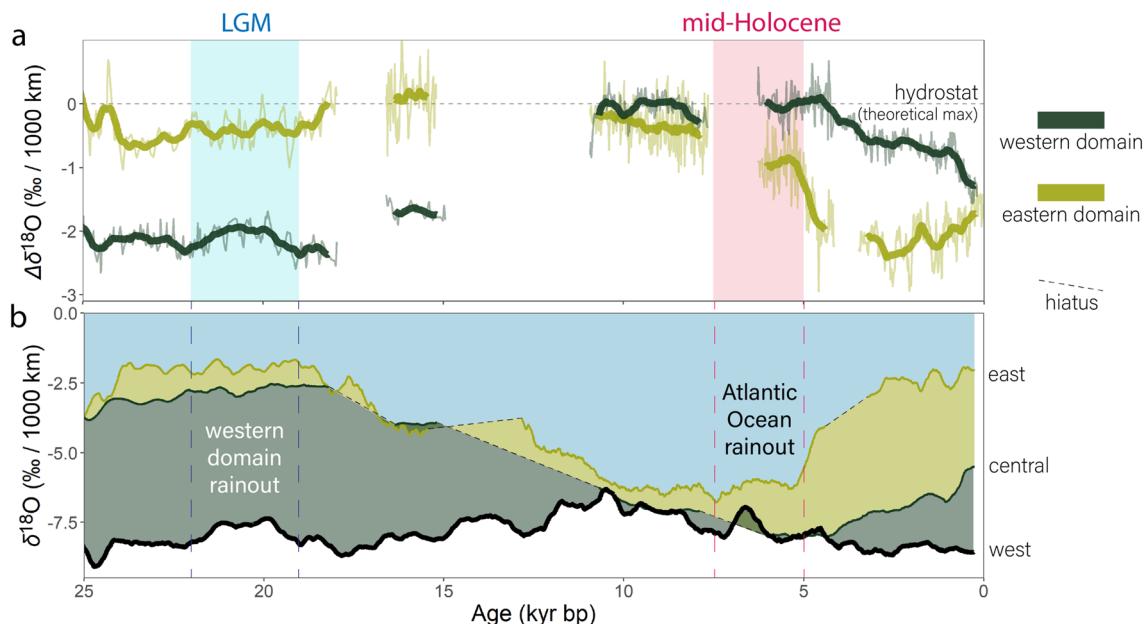
Figure 3. *Isotope gradient and individual* $\delta^{18}O$ *records.* (a) Eastern-to-central (light green) and central-to-western (dark green) isotopic gradients. More negative $\Delta\delta^{18}O$ is interpreted as more rainout between sites (wetter). (b) The three, smoothed $\delta^{18}O$ records (labels on right of panel) (Cheng et al., 2013; Cruz et al., 2009; van Breukelen et al., 2008; Wang et al., 2017). *Y*-axis color range is proportional to net moisture loss (rainout) within the western (dark green), eastern (light green), or ocean (turquoise) domains. The increase in blue toward the MH reflects a hypothesized increase in rainout over the ocean. Dashed lines are hiatus periods in the $\delta^{18}O$ records.

and was previously argued to contribute to the zonally imbalanced $\delta^{18}O$ signals by decreasing $\delta^{18}O$ everywhere, amplifying the eastern and dampening the western trend (Cheng et al., 2013). However, because this mechanism affects all sites similarly it cannot explain the $\Delta\delta^{18}O$ trends that we interpret as changes in the precipitation centroid's location.

4. Results and Interpretation

4.1. Isotope Gradients and Net Rainout

The isotope gradients over space are distinct from any one $\delta^{18}O$ record, suggesting there is no single representative site that reflects basin-wide rainout. Figure 3a shows these gradients for the eastern-to-central sites ("eastern domain"; light green) and central-to-western sites ("western domain"; dark green), with the theoretical maximum $\Delta\delta^{18}O$ value of zero labeled as the hydrostat (Caves et al., 2015; Chamberlain et al., 2014; Kukla et al., 2019). The hydrostat is the point where further drying has no affect on $\Delta\delta^{18}O$ because nearly all precipitation is being recycled. The eastern domain gradient is near the hydrostat from the LGM to the early Holocene, then decreases to ~−2.5‰ in the mid-late Holocene and increases by <1‰ to present. While at the hydrostat, $\Delta\delta^{18}O$ does not capture further drying that likely distinguishes the early mid Holocene conditions from the mid-late Holocene (P. A. Baker, Seltzer, et al., 2001; Cheng et al., 2013; Fritz et al., 2004; Kukla et al., 2021). The western domain gradient shows a mostly opposing trend, with $\Delta\delta^{18}O$ near ~−2‰ at the LGM and increasing to zero, the hydrostat, by the mid-Holocene before decreasing to present. The late Holocene $\Delta\delta^{18}O$ value in this domain is similar to the rainfall $\Delta\delta^{18}O$ across the tropical South America today (Salati et al., 1979; Wang et al., 2017). Overall, despite $\delta^{18}O$ shifts that are zonally imbalanced (about twice as large in the eastern and central records compared to the west), the magnitude of $\Delta\delta^{18}O$ change is comparable in each domain, consistent with zonally balanced changes in rainout.

Following previous work using isotope gradients (Hu et al., 2008; Salati et al., 1979; Winnick et al., 2014), we interpret the $\Delta\delta^{18}O$ data as reflecting rainout between two sites and the $\delta^{18}O$ data as recording the net integrated upwind rainout signal. Figure 3b is an attempt to visualize both the local ($\Delta\delta^{18}O$) and upwind ($\delta^{18}O$) rainout signals. Here, the eastern, central, and western $\delta^{18}O$ records are smoothed and plotted together with the space
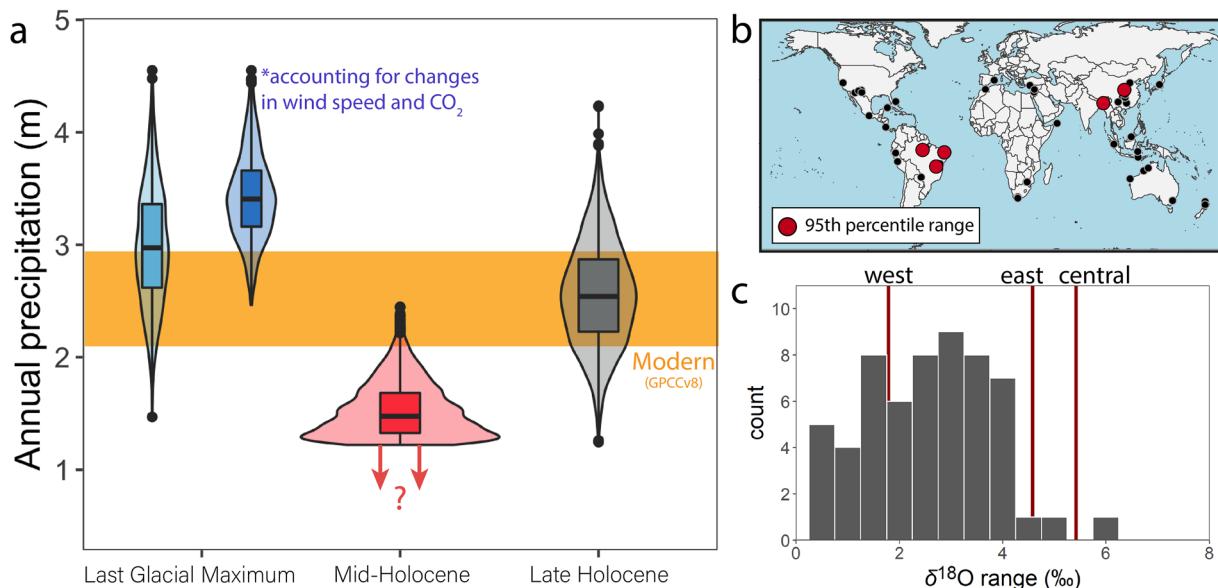
Figure 4. (a) Reconstructed precipitation for the Last Glacial Maximum (blue), mid-Holocene (red), and late Holocene (gray). Mid-Holocene is restricted at the lower-bound because $\Delta\delta^{18}O$ is at the hydrostat. (b) Map of records with $\delta^{18}O$ ranges in the largest 5% (red) and all sites (black). (c) The distribution of $\delta^{18}O$ ranges. Red, vertical lines show values for the west, central, and western sites discussed in the text. The central and eastern records are in the largest 5% of all similar sites (Text S4 in Supporting Information S1).

between them colored to illustrate the magnitude of change in $\delta^{18}O$ between each site. This figure shows that the location where $\delta^{18}O$ decreases the most (indicative of the most rainout) shifts from the western domain (dark green) at the LGM to east of the eastern site, over the tropical Atlantic Ocean (blue), by the mid-Holocene, to somewhere in between by the late Holocene.

This interpretive framework explains how the SAPD is zonally balanced despite zonally imbalanced $\delta^{18}O$ records. The western $\delta^{18}O$ shifts are small compared to the eastern record because the focus of rainout is always upwind of the western site. In contrast, the focus of rainout is downwind of the eastern and central sites at the LGM, and upwind of these sites at the mid-Holocene. Put otherwise, the focus of rainout shifts along the moisture trajectory relative to the eastern and central sites, but not the western site, driving larger amplitude $\delta^{18}O$ trends in the eastern and central sites. We note that additional complications at the eastern site, such as competing air-masses (Garreaud et al., 2009; Liu & Battisti, 2015) could modify the relationship between rainout and $\Delta\delta^{18}O$ through time. We caution against interpreting eastern $\Delta\delta^{18}O$ as quantitative trends in rainout, and we expand on this point in Section 5.4.

In addition to the zonally imbalanced $\delta^{18}O$ trends, another enigmatic feature of the $\delta^{18}O$ data is that the records are out-of-phase with one another. The out-of-phase nature of these $\delta^{18}O$ shifts can also be understood in the context of upwind effects. The western $\delta^{18}O$ record decreases from 10 to 5 ka (Figure 3b) while $\Delta\delta^{18}O$ stays near the theoretical maximum value of zero (Figure 3a), consistent with the $\delta^{18}O$ shift being driven by upwind rather than local rainout. Meanwhile, in the last 5 kyr, the focus of decreasing $\delta^{18}O$ shifts inland, first over the eastern domain and next over the western domain, revealing a time-transgressive trend that emerges from the central $\delta^{18}O$ data lagging the eastern record. Thus, the progressive inland migration of the focus of rainout provides a plausible mechanism for the enigmatic lag between these records.

4.2. Reconstructed Annual Precipitation Rates

Our reactive transport results suggest that late Holocene precipitation rates were similar to modern, consistent with similar $\Delta\delta^{18}O$ values between the late Holocene speleothem data and modern rainfall. During the LGM, we find increased rainfall relative to the late Holocene (light blue distribution of Figure 4a; $3,000 \pm 800$ mm/yr). This result is consistent with extensive evidence for wetter conditions in western tropical South America (P. A. Baker, Seltzer, et al., 2001; P. A. Baker, Rigsby, et al., 2001; Fritz et al., 2004). When wind speed and transpiration are

equal to or greater than modern values (see Section 3), calculated rainfall increases to ~3,400 ± 400 mm/yr to compensate for increased moisture transport and decreased isotopic fractionation associated with transpiration (dark blue distributions of Figure 4a). We note that hydrogen isotope composition (δD) of leaf waxes from the Amazon River appears higher at the LGM than before or after, suggesting drier conditions than today (Häggi et al., 2017). However, the signal is small (about 1‰–2‰ in $\delta^{18}O$) and not inconsistent with our finding that the western domain $\Delta\delta^{18}O$ values are higher at the LGM compared to before and after.

During the mid-Holocene, the reactive transport model simulates rainfall decreasing to ~1,200 mm/yr (about half of modern; red distribution of Figure 4a). As discussed in Kukla et al. (2021), the $\Delta\delta^{18}O$ values in the mid-Holocene straddle zero—the theoretical maximum value for a single moisture trajectory. At this point, further drying has a negligible effect on $\Delta\delta^{18}O$. The shape of the mid-Holocene distribution thus reflects the imposed lower-bound of annual precipitation, effectively restricting the solution to the wettest scenarios.

One limitation to our analysis is that we do not explicitly account for the possibility that changes in the seasonality of rainfall affects one site more than the other. Seasonality could be an issue in northeastern Brazil, where peak precipitation is offset from the central and western sites. However, seasonality, independent of rainout, is unlikely to drive the eastern (or central) $\delta^{18}O$ data because the amplitude of change is equal to or greater than the amplitude of $\delta^{18}O$ seasonality today (see Figure S4 in Supporting Information S1). To formalize this point, we use high and low austral summer insolation results for northeastern Brazil from the isotope-enabled GCM experiments of Liu and Battisti (2015) to show that a 5‰–8‰ decrease in wet-season precipitation $\delta^{18}O$ is required to explain the low mid-Holocene values (Text S6 and Figure S8 in Supporting Information S1). Changes in monthly precipitation amount have a small effect on annual $\delta^{18}O$, as noted by Liu and Battisti (2015), indicating that a shift in the dominant air-mass cannot explain the speleothem signal. This required decrease in wet-season $\delta^{18}O$ is about four times greater than that simulated by the isotope-enabled GCM (Figure S8 in Supporting Information S1). Given the small influence of precipitation and air-mass changes, it is best explained by an increase in net upwind rainout. We expand on how changes in seasonality and atmospheric circulation affect our conclusions at other sites in the discussion section.

The reactive transport model estimates of past precipitation show larger SAPD anomalies than predicted by GCMs (Cruz et al., 2009; Liu & Battisti, 2015; Shimizu et al., 2020). GCM simulations of the SAPD have accounted for precession and its impact on land surface heating, but not other "boundary condition" changes such as the land albedo response to vegetation change. If the speleothem $\delta^{18}O$ data reliably reflects past precipitation $\delta^{18}O$, we must consider the possibility that other factors, in addition to (and in response to) precession, shape the late Quaternary SAPD.

Zonal migration of the precipitation centroid should drive larger precipitation anomalies than a zonally static precipitation centroid. Battisti et al. (2014), for example, argues that a zonal shift in the pan-Asian monsoon with changing northern hemisphere summer insolation could explain some of the largest documented speleothem $\delta^{18}O$ shifts. Using the SISALv2 database (Atsawawaranunt et al., 2018; Comas-Bru et al., 2019, 2020) we find that magnitude of $\delta^{18}O$ shifts in the eastern and central records is in the top 5% of all comparable records (duration between 10^3 and 10^5 years and within 40° of the equator) (see Text S4 in Supporting Information S1) (Figures 4b and 4c). The other records with large $\delta^{18}O$ ranges appear near the pan-Asian monsoon region, consistent with these two regions being among the most sensitive to zonal energy anomalies and precipitation shifts (Battisti et al., 2014; Boos & Korty, 2016).

4.3. PMIP3/CMIP5 Analysis With Energy Balance and Reactive Transport Models

Our analyses with the PMIP3/CMIP5 data affirm previous isotope-enabled GCM results (Cruz et al., 2009; Liu & Battisti, 2015). The simulations do not capture zonal migration of the precipitation centroid and they under-estimate the magnitude of $\delta^{18}O$ variation. We find that, while the EFE shifts northward in the mid-Holocene wet season (a result contested by other models, Liu and Battisti (2015) and Chiessi et al. (2021)), the EFPM does not show any systematic shift to the east or west (Figure 5a). Meanwhile, when forced with PMIP3/CMIP5 output the reactive transport model correctly predicts late Holocene $\Delta\delta^{18}O$ data, demonstrating that the net rainout in the models is consistent with the isotope data despite broad precipitation biases. During the LGM, however, the PMIP3/CMIP5 output leads to an isotope gradient that is too shallow, consistent with the models being too dry (Figures 5b and 5c). In contrast, the simulated isotope gradients are too steep at the mid-Holocene when driven by
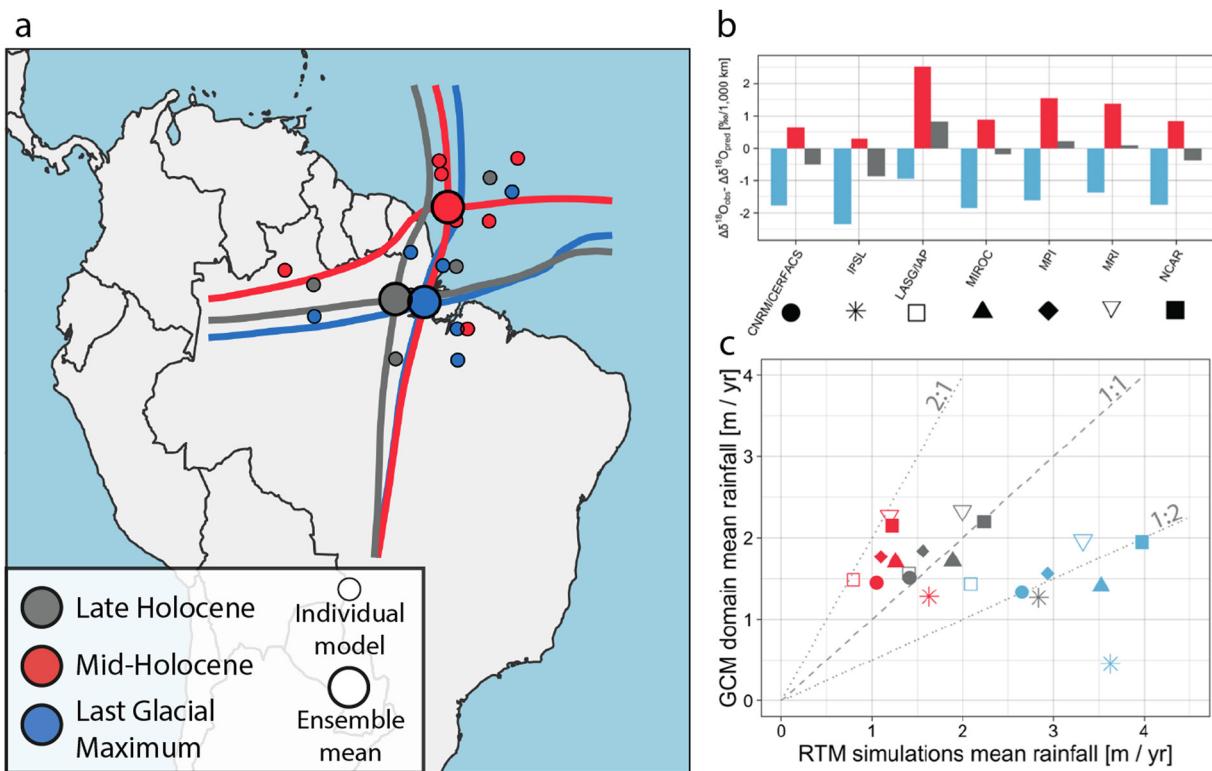
Figure 5. *PMIP3/CMIP5 SAM centroid and isotope gradient analysis.* (a) PMIP3 models show little zonal variation in the tropical South American precipitation centroid from the Last Glacial Maximum (LGM), mid-Holocene, and late Holocene (pre-industrial) for months NDJFMAM. (b) When forced with PMIP3/CMIP5 output, the reactive transport model (Kukla et al., 2019) systematically predicts a steeper-than-observed δ¹⁸O gradient at the mid-Holocene (red bars) and a shallower-than-observed gradient at the LGM (blue bars) with no systematic error in the late Holocene. This result is consistent with the δ¹⁸O error found in the isotope-enabled simulations of Cruz et al. (2009) and Liu and Battisti (2015). (c) To match the observed oxygen isotope gradient, the reactive transport model requires similar rainfall amounts as predicted by the PMIP3/CMIP5 models at the late Holocene, but requires drier conditions than PMIP3/CMIP5 at the mid-Holocene and wetter conditions at the LGM.

PMIP3/CMIP5 output, consistent with the models being too wet. Taken together, zonal shifts in the precipitation centroid are negligible in the PMIP3/CMIP5 models and their precipitation anomalies are smaller than suggested by the isotope data, despite good agreement in the late Holocene.

We therefore hypothesize that the zonal migration of the precipitation centroid can resolve these discrepancies. This hypothesis is outlined in Figure 6, and we address its plausibility in the following subsection. We hypothesize that the precipitation centroid tracks the region of maximum net rainout (decreasing δ¹⁸O), located between the central and western records at the Last Glacial Maximum (Figures 6c and 6f), upwind of the eastern record at the mid-Holocene (Figures 6b and 6e), and somewhere in between in the late Holocene (Figures 6a and 6d), consistent with its modern position (Boos & Korty, 2016). While zonal precipitation centroid migration aligns with the δ¹⁸O data and its magnitude of change, it is unclear whether late Quaternary forcings could plausibly drive such zonal shifts.

4.4. Zonal Migration of the Precipitation Centroid in an Energy Balance Model

We find that reasonable zonally asymmetric forcings for the mid-Holocene and LGM, not captured in the PMIP3/CMIP5 models, can cause the precipitation centroid to shift zonally relative to its initial PMIP3/CMIP5 ensemble mean state (Figure 7). In our energy balance model simulations, the anomalous MSE source owed to a darker Sahara at the mid-Holocene is sufficient to pull the EFPM east of the eastern speleothem record, consistent with its mid-Holocene δ¹⁸O minimum (Figures 7d–7f). In contrast, a decrease in forest cover in tropical Africa and Eurasia pushes the EFPM westward in the LGM (Figures 7a–7c). We note that the location of the EFE-prime meridian intersection approximates, but may be offset from, the location of the precipitation centroid (Boos & Korty, 2016), although this offset should be constant as the precipitation centroid migrates (Adam et al., 2016;
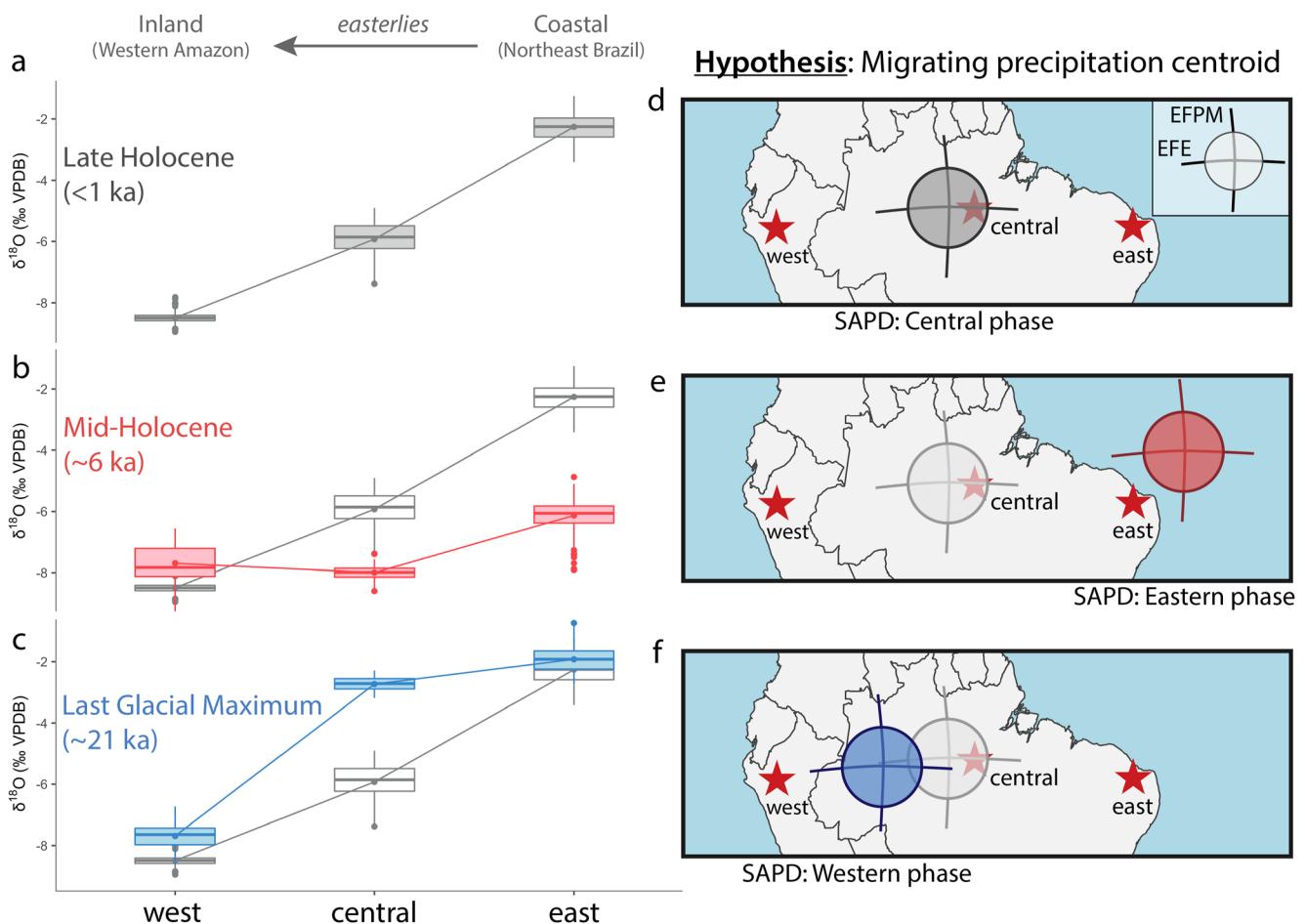
Figure 6. *Precipitation centroid migration hypothesis and its isotopic expression.* (a–c) Show the three distinct isotope profiles of the (a) late Holocene, (b) mid-Holocene, and (c) Last Glacial Maximum (LGM). Late Holocene is reproduced in panels (b and c) for comparison. Lines connect the mean of each site. Data from van Breukelen et al. (2008), Cruz et al. (2009), Cheng et al. (2013), and Wang et al. (2017). (d–f) Illustrate hypothesized changes in the South American precipitation centroid (intersection of the energy flux equator and energy flux prime meridian) based on where most of the $\delta^{18}O$ decrease (rainout) occurs (tropical Atlantic/northeast Brazil at mid-Holocene, and western Amazon at LGM).

Boos & Korty, 2016). The simple energy balance model does not account for changes in the partitioning between latent and sensible heat, but any repartitioning does not alter the total energy flux from the land to the base of the atmospheric column (Laguë et al., 2019). Instead, repartitioning could affect the net energy imbalance via uncertain cloud feedbacks (Laguë et al., 2021) and possibly amplify the imbalance due to latent cooling-driven reductions in outgoing longwave radiation (Boos & Korty, 2016). A decrease in Saharan dustiness would also amplify the energy imbalance, though we do not account for it here. Our analysis shows that the precipitation centroid is sufficiently sensitive to remote forcing to explain the late Quaternary precipitation anomalies, although the exact location of rainout will depend on the initial state (here, from PMIP3/CMIP5) and the relative offset between the energy flux intersection and the precipitation centroid.

5. Discussion

5.1. A Zonally Balanced SAPD

Previous work has argued that the distinct trends between the western and central/eastern $\delta^{18}O$ data reflect either (a) a zonally imbalanced precipitation dipole (Cheng et al., 2013); or (b) changes in the strength of convection, but not the location of peak rainout (Wang et al., 2017). Here, we address how our results support a third scenario—a zonally balanced SAPD that reconciles the zonally imbalanced amplitudes of $\delta^{18}O$ change. We also discuss how accounting for upwind rainout distinguishes our revised $\delta^{18}O$ interpretations from previous work.
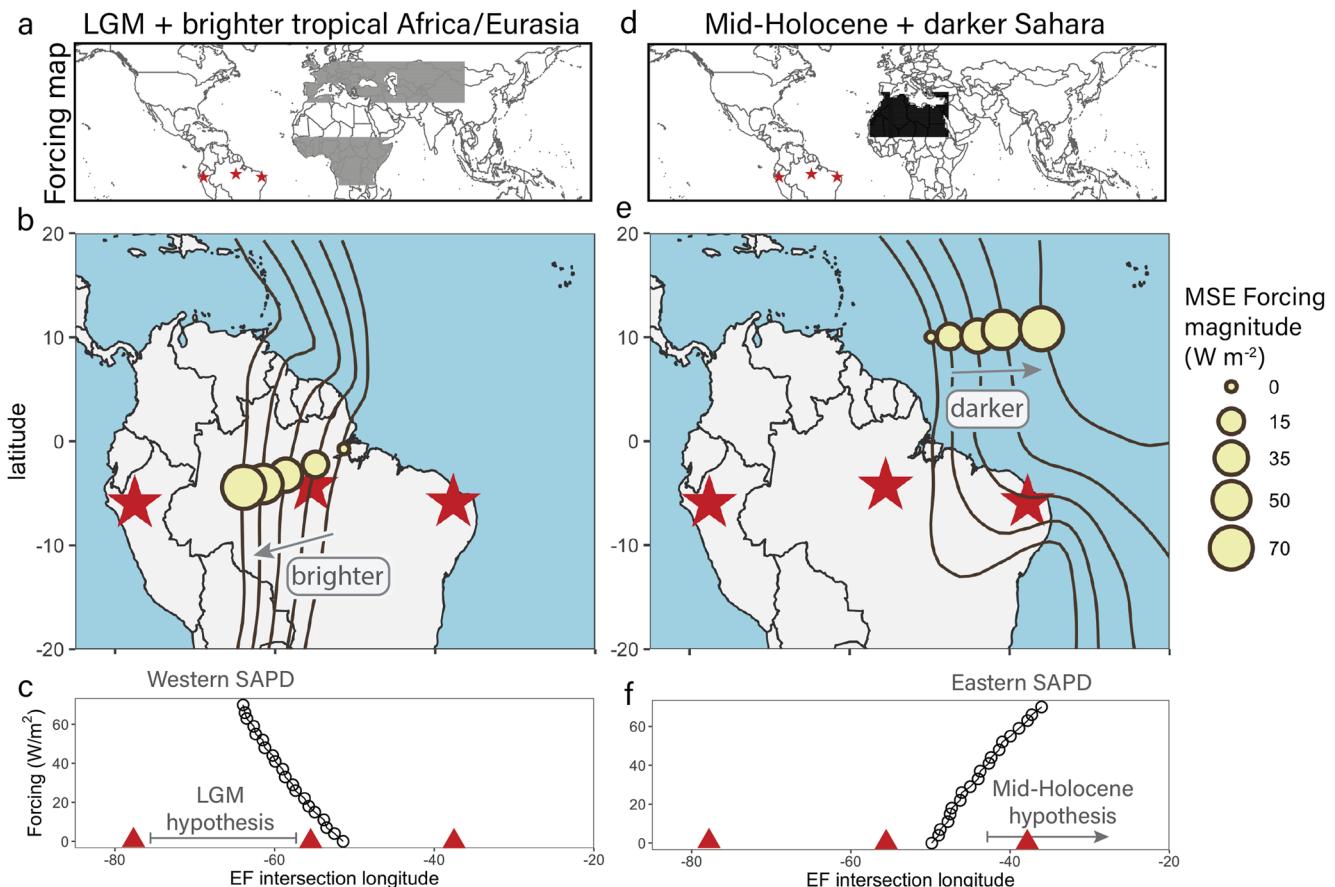
Figure 7. *Sensitivity of the South American Precipitation Dipole to zonal energy anomalies.* Gray and black boxes in the maps of panels (a, d) show the locations of Last Glacial Maximum (LGM) and mid-Holocene moist static energy forcings, respectively. Panels (b, e) show the response of the energy flux prime meridian (lines) and energy flux intersection (points; approximating the precipitation centroid) to selected forcing levels for the LGM and mid-Holocene. The energy flux intersection longitude versus the magnitude of forcing is shown in panels (c, f) for the LGM and mid-Holocene. We note that the points on the map panels are not a proposed path of the precipitation centroid in the late Quaternary, but rather the response to different forcing magnitudes starting from the PMIP3/CMIP5 initial conditions.

Larger $\delta^{18}O$ signals in the eastern and central records do not require larger precipitation anomalies because a shift in the location of peak rainout has a small effect on sites that remain downwind. That is, whether the focus of rainout occurs near the speleothem site or a few hundred kilometers upwind, speleothem $\delta^{18}O$ will be approximately the same as long as the same magnitude of rainout occurs before the airmass reaches that site. We argue that this is why the western $\delta^{18}O$ trends are muted—the focus of rainout remains upwind of the western site for the entirety of the record. This may also explain discrepancies with basin-integrated precipitation isotope data. Häggi et al. (2017), for example, find basin-integrated δD trends that are small (~1‰–2‰ in $\delta^{18}O$) and distinct from any one speleothem $\delta^{18}O$ record in the last 50 kyr, consistent with a decoupling of $\delta^{18}O$ and local precipitation amount. The magnitude of total rainout, and basin-integrated precipitation $\delta^{18}O$, appear relatively constant through time, regardless of whether that rainout occurs in the west or east. The western and eastern legs of the SAPD are approximately balanced.

Previous work has applied a different interpretive framework to the central and western $\delta^{18}O$ data to argue that the Amazon was wetter in the mid-Holocene and drier at the LGM, opposing our results (Wang et al., 2017). The key distinction with our work is that Wang et al. (2017) assume that upwind $\delta^{18}O$ is constant (with corrections for temperature and seawater $\delta^{18}O$ following P. A. Baker and Fritz (2015)) such that the central $\delta^{18}O$ record drives all variability in $\Delta\delta^{18}O$. We argue that the assumption of an effectively constant upwind $\delta^{18}O$ value is refuted by data (Cruz et al., 2009)—the strong correlation between central and eastern (upwind) $\delta^{18}O$ records is evidence that upwind $\delta^{18}O$ is propagating downwind without attenuation. Our approach avoids the assumption that upwind moisture loss is constant through time and, as we discuss in the next section, is consistent with evidence that $\delta^{18}O$ is not always strongly coupled with *local* precipitation amount (Ward et al., 2019; Wortham et al., 2017). Within
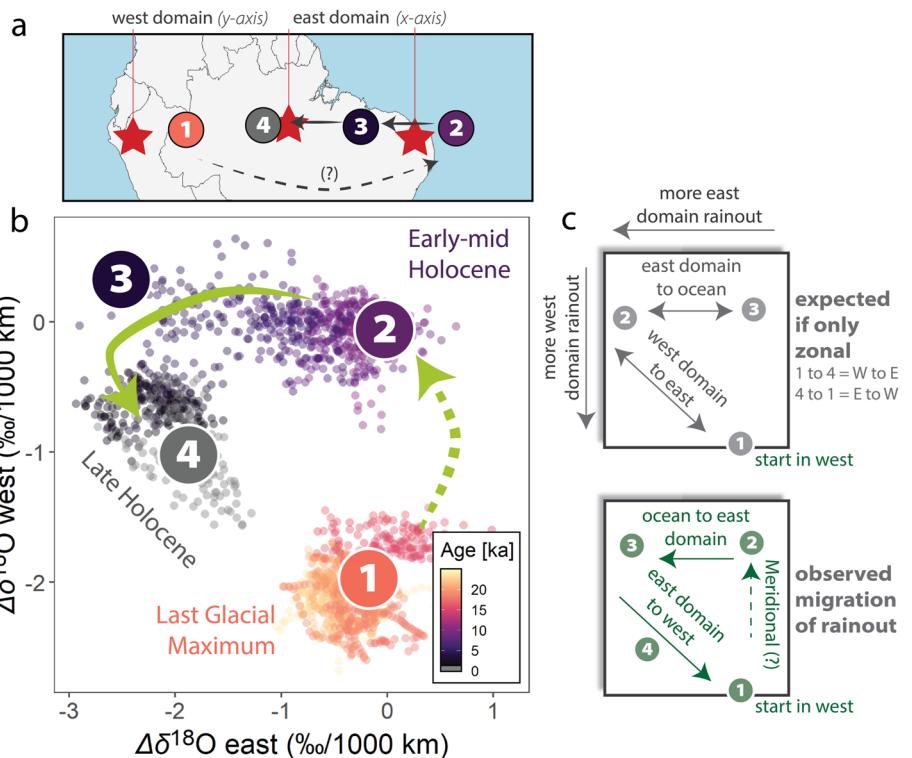
Figure 8. *Isotope gradients reflect zonal and meridional shifts in the precipitation centroid.* (a) Map of speleothem sites showing the east and west domains—the axes of panel (b)—and a schematic for the interpretation of panel (b). (b) Crossplot of eastern and western domain data (derived from data in van Breukelen et al. (2008), Cruz et al. (2009), Cheng et al. (2013), and Wang et al. (2017)). Numbered points in panel (b) correspond with numbers in panels (a, c). (c) More negative $\Delta\delta^{18}O$ refers to more rainout in a given domain. Data should track a sideways "V" shape if the focus of rainout migrates only zonally (top panel, note different order of numbers). However, the Last Glacial Maximum to early mid Holocene does not follow this zonal trajectory, suggesting a meridional component (dashed arrow).

our framework, the wettest time occurs when the isotope gradient is steepest, not when central $\delta^{18}O$ is lowest, consistent with our understanding of how $\Delta\delta^{18}O$ relates to precipitation today (Ampuero et al., 2020; Pattnayak et al., 2019; Salati et al., 1979).

5.2. Zonal and Meridional Components of Precipitation Centroid Migration

Late Quaternary forcings, including precession and land surface change, should lead to zonal and meridional shifts in the precipitation centroid. The EFE drives north-south migration that is well-documented in late Quaternary proxy records (Arbuszewski et al., 2013; Chiessi et al., 2021; Deplazes et al., 2013; Mulitza et al., 2017), and the EFPM drives the east-west component (Boos & Korty, 2016) which we argue is evident in the speleothem $\delta^{18}O$ data. Because the location of the precipitation centroid varies near-linearly with anomalous forcing (rather than abruptly at some threshold; Figure 7) its spatial migration should cause time-transgressive proxy trends as it reaches different locations at different times. Here, we compare the west-east (LGM to mid-Holocene) and east-west (mid-Holocene to present) SAPD transitions and discuss evidence for zonal and meridional structure of precipitation centroid migration with asynchronous proxy signals, consistent with our hypothesis.

We first focus on a broad comparison of the two SAPD transitions by comparing the eastern-to-central (eastern domain) and central-to-western (western domain) $\Delta\delta^{18}O$ data, shown in Figure 8b. Here, lower values on the y-axis are interpreted as more western domain rainout, and lower values on the x-axis as more eastern domain rainout. If the focus of rainout only migrates zonally, then a west-east trade-off in rainout will mark a diagonal line with slope −1 (as rainout in one domain increases at the expense of the other), and a shift in rainout further east over the ocean will trace a flat line with an intercept near zero (no rainout in the western domain, only moving through the eastern domain) (Figure 8c, "expected if only zonal"). The $\Delta\delta^{18}O$ data, however, do not

follow this trend. Instead, the LGM to early mid Holocene marks a decrease in western domain rainout (increase in y-axis) with no compensating increase in the east (x-axis remains near zero) (Figure 8b, points 1–2), followed by a mostly zonal progression into the eastern, then western domain (points 2–3 and 3–4, respectively). The precipitation centroid appears to migrate eastward with a meridional component relative to the speleothem sites from the LGM to early mid Holocene, and then westward following a zonal pattern through the speleothem sites to present.

This inferred pattern of migration from the $\Delta\delta^{18}O$ data is supported by independent proxy results. In the last 8,000 years, for example, a steeper isotope gradient reflecting more moisture distillation first appears in the eastern domain from ∼8–5 ka (points 2–3 of Figure 8), and next in the western domain from ∼5–0 ka (points 3–4) (see also Figure 3). This result suggests that the precipitation centroid began passing over the central record ∼5,000 years ago, consistent with recent strontium isotope evidence from the same site pointing to high infiltration rates from 6 to 5 ka with less infiltration before and after (Ward et al., 2019). The timing of migration is also consistent with a shift from dry to wet conditions in a nearby lake (Reis et al., 2017). After ∼5 ka, rainfall begins increasing in the western domain and water infiltration rates at the central site temporarily decline (Ward et al., 2019). As discussed earlier, this gradual westward migration of rainout also explains the perplexing lag of central $\delta^{18}O$ behind the eastern record (Figures 1c and 1d). The precipitation centroid first reaches the eastern site at ∼8–7 ka when $\delta^{18}O$ values are lowest, and later the central site at ∼5 ka, in tandem with records of the local water balance (Reis et al., 2017; Ward et al., 2019).

Unlike this east-west migration, the dipole transition from west to east spanning ∼20–10 ka does not coincide with a decrease in eastern domain $\Delta\delta^{18}O$, and we suggest this reflects the precipitation centroid moving around, rather than through, the eastern domain (points 1–2 of Figure 8). Movement around the domain would require a meridional component of precipitation centroid migration reflected by a change in $\Delta\delta^{18}O$ in one domain that is not balanced by a corresponding change in the other (Figure 8c, bottom panel). It is possible that the precipitation centroid moved southeast around the central $\delta^{18}O$ site as there is evidence for wetter conditions to the southeast (Fornace et al., 2016; Whitney et al., 2011) and drier conditions to the north (Deplazes et al., 2013; Zular et al., 2019), as well as some evidence for a south-shift of the EFE (Arbuszewski et al., 2013). The southeast appears to become drier around 12 ka, approximately when a nearby speleothem $\delta^{18}O$ shift occurs that is consistent with decreased Amazon and more Atlantic-derived moisture (Figure S9 in Supporting Information S1) (Novello et al., 2017, 2018).

As the precipitation centroid migrates further east, after ∼12 ka, pollen data from semi-arid northeastern Brazil (near the eastern $\delta^{18}O$ site) suggest humid conditions from ∼10.9–6.7 ka (De Oliveira et al., 1999). Humidity peaks halfway through this interval (∼8.9 ka) when eastern $\delta^{18}O$ reaches its lowest values (Cruz et al., 2009; De Oliveira et al., 1999), suggesting this marks the easternmost extent and turning point of the precipitation centroid. As discussed earlier, this timing also corresponds with the onset of the time-transgressive westward shift in wet conditions that continues to the present. While more work is needed to trace the past focus of rainfall, we suggest the progressive shifts in wet conditions across the continent (both east-west and west-east) provide empirical support and a testable framework for the pattern of precipitation centroid migration.

5.3. Mechanisms for Zonal Precipitation Centroid Migration

While climate model simulations are necessary to assess the dynamical drivers of precipitation centroid migration, our analysis allows us to present testable hypotheses. For example, the greening of the Sahara at the mid-Holocene (about 70 W/m² anomalous heat source at top of atmosphere; Boos and Korty (2016)) is likely sufficient to drive the EFPM eastward entirely over the tropical Atlantic (Figures 7e and 7f). Comparison to proxy records from Africa generally support this remote influence on tropical South American rainfall. Dust flux records of West African Monsoon behavior show pronounced precession-scale variability in the last 240 kyr with prominent exceptions at ∼30, ∼70, and ∼150 ka when dust fluxes "skip" precession beats (Skonieczny et al., 2019). In South America, western Amazon $\delta^{18}O$ records lose sensitivity to precession at the same times (and $\Delta\delta^{18}O$ where there is data, in the ∼30 ka case; Figure S10 in Supporting Information S1) (Cheng et al., 2013; Mosblech et al., 2012; Wang et al., 2017). Further, there is a rapid increase in $\delta^{18}O$ at the eastern site at ∼5 ka, consistent with a westward (inland) shift of rainout, contemporaneous with the termination of the African Humid Period in North Africa (Shanahan et al., 2015) where increasing land albedo would provide an anomalous energy sink. These similarities are mostly preliminary and more data is needed to test if they hold over space and time, but they are consistent with expectations if the zonal location of the precipitation centroid was sensitive to Saharan albedo.

At the LGM, vegetation change that increases land albedo in tropical Africa and Eurasia could push the EFPM westward. However, it is not clear if the magnitude of forcing required for this shift could be accomplished by the LGM vegetation change alone. For example, low $\Delta\delta^{18}O$ values (along with high runoff (Nace et al., 2014)) are a persistent feature in the western domain for at least ~20 kyr before the LGM (Figure S10 in Supporting Information S1), suggesting the cause of a westward shift in rainout is not unique to this time interval. African dust fluxes were persistently high from 40 to 20 ka, consistent with a remote albedo forcing, but data for other possible drivers of precipitation centroid migration, such as the strength of the easterlies, is sparse at this time.

Based on the zonal, meridional, and hysteresis-like migration of the South American precipitation centroid, we suggest that multiple forcing mechanisms operate at different times to drive these complex, precession-scale patterns. Remote land albedo change could play a particularly important role in driving zonal shifts in rainout, but more sophisticated climate model simulations are needed to rigorously test these hypotheses. We note that Heinrich and Dansgaard/Oeschger events are also linked to remote forcing of tropical South American precipitation (Arz et al., 1998; Kanner et al., 2012; Nace et al., 2014), but these shorter, millennial-scale events are beyond the scope of this study.

5.4. Air-Mass and Seasonality Complications

Up to now, our interpretation of a zonal shift in the precipitation centroid has hinged on the assumption that the three speleothem sites are isotopically connected through time. Here, we discuss how relaxing this assumption does not necessarily invalidate our conclusions. This assumption warrants scrutiny because, at least in the eastern-to-central record domain, the timing of peak precipitation and the relevant air-mass can differ between sites (Figure S4 in Supporting Information S1, Garreaud et al. (2009) and Liu and Battisti (2015)) suggesting the isotopic connection may not be strong through time.

For simplicity, we consider two forms of isotopic connectivity between sites: (a) an "air-mass connection," where the same air mass rains out at both sites and (b) a "recycling connection" where rainout at one site evaporates and re-precipitates at the other. An air-mass connection implies a recycling connection and allows upwind isotopic signals to propagate fully downwind. When two sites share only a recycling connection, each site is dominated by a different air-mass and the upwind signal propagates downwind with some attenuation due to air-mass mixing. While changes in circulation might alter the strength of the air-mass connection across tropical South America through time, the recycling connection is likely more robust. For example, about half of western Amazon rainfall is derived from upwind recycling (Staal et al., 2018; Zemp et al., 2017) and upwind (northeastern Brazil) transpiration can travel over 1,000 km before re-precipitating out, connecting the east and west (Staal et al., 2018).

First, we note that if two sites share an air-mass and recycling connection, then the mean isotope gradient is insensitive to differences in the timing of peak precipitation between them. We demonstrate this point with a toy model that simulates the isotope gradient between two sites that have different phases of precipitation seasonality (Text S5 in Supporting Information S1). Differences in the seasonal phase lead to $\Delta\delta^{18}O$ errors (relative to the in-phase case), but these errors are negligible—less than 1% of the seasonal $\Delta\delta^{18}O$ amplitude (Figures S11 and S12 in Supporting Information S1). Thus, a difference in the timing of peak precipitation—as between the eastern and central sites—does not, itself, invalidate the $\Delta\delta^{18}O$ framework.

Still, our conclusions could be impacted if the air-mass connection between sites is weak at some point in time. We evaluate two additional scenarios that address this possibility. First, we assume there is a weak air-mass connection between the eastern and central sites. In this case, the high-$\delta^{18}O$ values at these sites during the LGM indicate that their air-masses are delivering undistilled moisture. The precipitation centroid—where moisture distillation is strongest—is likely situated to the west. Toward the mid-Holocene, eastern and central $\delta^{18}O$ decrease in tandem, with no evidence for the downwind attenuation that is expected if upwind recycling was mixing with an independent air-mass. Perhaps $\delta^{18}O$ of the central site's air-mass also decreased from the LGM to mid-Holocene, hiding the attenuation. In this case, lest we invoke a third air-mass somehow, the central signal should propagate west. Wang et al. (2017) explain the lack of western signal by invoking an increase in plant transpiration, but this mechanism has been discredited (Ampuero et al., 2020; Pattnayak et al., 2019).

In the alternate scenario, we assume the eastern and central sites share an air-mass connection with each other, but not the western site. In this case, the eastern and central $\delta^{18}O$ shift from the LGM to mid-Holocene makes sense, however it is not consistent with the lack of a signal in the west. The signal could be masked by a

coincident decrease in the western air-mass's rainout, but such a decrease may also be related to a zonal shift in the precipitation centroid. Still, western $\delta^{18}O$ shifts directions to track the central site as soon as $\Delta\delta^{18}O$ reaches the theoretical maximum value for two sites with a strong air-mass connection. Without a strong air-mass connection, this western $\delta^{18}O$ shift and the central and eastern $\delta^{18}O$ decrease after the LGM must be somewhat coincidental, driven by coeval changes in independent air-masses that happen to cancel out the attenuation of the upwind signal while obeying the theoretical maximum $\Delta\delta^{18}O$ of a single air-mass system. Arguments against a strong air-mass connection should address how these apparently unattenuated signals occur in the speleothem data. Overall, we argue that uncertainty in the strength of the air-mass connection makes our quantitative precipitation reconstruction less certain, but it does not conflict with our zonal precipitation centroid migration hypothesis.

6. Conclusion

Our analysis provides a path forward for resolving the enigmatic, non-uniform trends in tropical South American speleothem $\delta^{18}O$, but it rests on assumptions, many previously discussed, that deserve further scrutiny. One critical assumption that is difficult to address is that speleothem $\delta^{18}O$ reliably tracks precipitation $\delta^{18}O$ at all sites. Kinetic fractionation and other confounding processes could decouple speleothem and precipitation $\delta^{18}O$, challenging our model approach. Such effects have not been documented in these speleothems (Cheng et al., 2013; Cruz et al., 2009; van Breukelen et al., 2008; Wang et al., 2017), but additional proxy constraints (such as triple oxygen and mass-48 clumped isotopes) will provide more rigorous tests of local and kinetic effects (Huth et al., 2022). Another limitation lies in the simplified energy balance modeling approach. The goal of these model exercises is to present plausible drivers of zonal rainout shifts for further testing, while recognizing that our list of drivers is not exhaustive. Future studies of the SAPD with more sophisticated models should analyze the zonal location of the EFPM and its relation to zonal precipitation patterns to test whether this zonal precipitation centroid migration effect is present.

It is also fair to question whether the discrepancies between proxies and isotope-enabled GCMs are resolvable, as we posit. GCMs are known to struggle with tropical South American precipitation—there is substantial inter-model spread and dry-bias in seasonal and annual rainfall that complicate their application to exotic, paleoclimate states (Li et al., 2006; Ribas et al., 2022). However, these models show better agreement in their simulated precipitation change, and their precipitation biases do not appear to cause biases in net rainout (see Figure 5c). We also reiterate that, while we question whether precession without land albedo change sufficiently explains the late Quaternary SAPD, our work should not be taken to discredit the role of precession more generally. We expect that the spatial pattern and amplitude of $\delta^{18}O$ anomalies can vary from one precession cycle to the next, depending on how orbital forcing interacts with other forcings and feedbacks within the Earth system. A zonal shift in the precipitation centroid is not required to explain zonally opposing precipitation anomalies, but it helps explain certain features of the late Quaternary proxy data, including the zonally imbalanced amplitude of $\delta^{18}O$ change and their notable phase-shifted trends. Our results build on previous work (Battisti et al., 2014) suggesting that zonal forcings may help explain some of the enigmatic proxy records found in places where tropical precipitation is energetically primed to migrate east-west.

Conflict of Interest

The authors declare no conflicts of interest relevant to this study.

Data Availability Statement

Code and data associated with this study can be found through Zenodo (Kukla et al., 2022) and Github (https://github.com/tykukla/ZonalPrecipPatterns-Amazon). The Zenodo/Github repository includes code and results for the energy balance and reactive transport model analysis, SISALv2 analysis, speleothem $\delta^{18}O$ data cleaning and smoothing, and the proxy compilation in Figure 1 of the main text. We note that the Tigre Perdido record (van Breukelen et al., 2008) from the western composite data was downloaded from the SISAL database (siteID: 25) (Comas-Bru et al., 2022), while other speleothem records were provided by the original authors or taken from the supplementary materials of the relevant publication (Cheng et al., 2013; Cruz et al., 2009; Wang et al., 2017).

References

Abouchami, W., & Zabel, M. (2003). Climate forcing of the Pb isotope record of terrigenous input into the Equatorial Atlantic. *Earth and Planetary Science Letters*, *213*(3–4), 221–234. https://doi.org/10.1016/S0012-821X(03)00304-2

Adam, O., Bischoff, T., & Schneider, T. (2016). Seasonal and interannual variations of the energy flux equator and ITCZ. Part II: Zonally varying shifts of the ITCZ. *Journal of Climate*, *29*(20), 7281–7293. https://doi.org/10.1175/JCLI-D-15-0710.1

Adkins, J., de Menocal, P., & Eshel, G. (2006). The "African humid period" and the record of marine upwelling from excess [230]Th in Ocean Drilling Program Hole [658]C. *Paleoceanography*, *21*(4), PA4203. https://doi.org/10.1029/2005PA001200

Ampuero, A., Stríkis, N. M., Apaéstegui, J., Vuille, M., Novello, V. F., Espinoza, J. C., et al. (2020). The forest effects on the isotopic composition of rainfall in the northwestern Amazon basin. *Journal of Geophysical Research: Atmospheres*, *125*(4), e2019JD031445. https://doi.org/10.1029/2019JD031445

Arbuszewski, J. A., de Menocal, P. B., Cléroux, C., Bradtmiller, L., & Mix, A. (2013). Meridional shifts of the Atlantic intertropical convergence zone since the Last Glacial Maximum. *Nature Geoscience*, *6*(11), 959–962. https://doi.org/10.1038/ngeo1961

Arz, H. W., Pätzold, J., & Wefer, G. (1998). Correlated millennial-scale changes in surface hydrography and terrigenous sediment yield inferred from last-glacial marine deposits off northeastern Brazil. *Quaternary Research*, *50*(2), 157–166. https://doi.org/10.1006/qres.1998.1992

Atsawawaranunt, K., Comas-Bru, L., Mozhdehi, S. A., Deininger, M., Harrison, S. P., Baker, A., et al. (2018). The SISAL database: A global resource to document oxygen and carbon isotope records from speleothems. *Earth System Science Data*, *10*(3), 1687–1713. https://doi.org/10.5194/essd-10-1687-2018

Baker, J. C. A., Gloor, M., Spracklen, D. V., Arnold, S. R., Tindall, J. C., Clerici, S. J., et al. (2016). What drives interannual variation in tree ring oxygen isotopes in the Amazon?: What drives Amazon tree ring δ^{18}O? *Geophysical Research Letters*, *43*(22), 11831–11840. https://doi.org/10.1002/2016GL071507

Baker, P. A., & Fritz, S. C. (2015). Nature and causes of Quaternary climate variation of tropical South America. *Quaternary Science Reviews*, *124*, 31–47. https://doi.org/10.1016/j.quascirev.2015.06.011

Baker, P. A., Rigsby, C. A., Seltzer, G. O., Fritz, S. C., Lowenstein, T. K., Bacher, N. P., & Veliz, C. (2001). Tropical climate changes at millennial and orbital timescales on the Bolivian Altiplano. *Nature*, *409*(6821), 698–701. https://doi.org/10.1038/35055524

Baker, P. A., Seltzer, G. O., Fritz, S. C., Dunbar, R. B., Grove, M. J., Tapia, P. M., et al. (2001). The history of South American tropical precipitation for the past 25,000 years. *Science*, *291*(5504), 640–643. https://doi.org/10.1126/science.291.5504.640

Battisti, D. S., Ding, Q., & Roe, G. H. (2014). Coherent pan-Asian climatic and isotopic response to orbital forcing of tropical insolation. *Journal of Geophysical Research: Atmospheres*, *119*(21), 11997–12020. https://doi.org/10.1002/2014JD021960

Binney, H., Edwards, M., Macias-Fauria, M., Lozhkin, A., Anderson, P., Kaplan, J. O., et al. (2017). Vegetation of Eurasia from the Last Glacial Maximum to present: Key biogeographic patterns. *Quaternary Science Reviews*, *157*, 80–97. https://doi.org/10.1016/j.quascirev.2016.11.022

Boers, N., Rheinwalt, A., Bookhagen, B., Barbosa, H. M. J., Marwan, N., Marengo, J., & Kurths, J. (2014). The South American rainfall dipole: A complex network analysis of extreme events. *Geophysical Research Letters*, *41*(20), 7397–7405. https://doi.org/10.1002/2014GL061829

Boos, W. R., & Korty, R. L. (2016). Regional energy budget control of the intertropical convergence zone and application to mid-Holocene rainfall. *Nature Geoscience*, *9*(12), 892–897. https://doi.org/10.1038/ngeo2833

Braconnot, P., Harrison, S. P., Kageyama, M., Bartlein, P. J., Masson-Delmotte, V., Abe-Ouchi, A., et al. (2012). Evaluation of climate models using palaeoclimatic data. *Nature Climate Change*, *2*(6), 417–424. https://doi.org/10.1038/nclimate1456

Bradtmiller, L. I., McGee, D., Awalt, M., Evers, J., Yerxa, H., Kinsley, C. W., & de Menocal, P. B. (2016). Changes in biological productivity along the northwest African margin over the past 20,000 years. *Paleoceanography*, *31*(1), 185–202. https://doi.org/10.1002/2015PA002862

Brienen, R. J. W., Helle, G., Pons, T. L., Guyot, J.-L., & Gloor, M. (2012). Oxygen isotopes in tree rings are a good proxy for Amazon precipitation and El Niño-Southern Oscillation variability. *Proceedings of the National Academy of Sciences of the United States of America*, *109*(42), 16957–16962. https://doi.org/10.1073/pnas.1205977109

Campos, J. L. P. S., Cruz, F. W., Ambrizzi, T., Deininger, M., Vuille, M., Novello, V. F., & Strikis, N. M. (2019). Coherent South American Monsoon variability during the last Millennium revealed through high-resolution proxy records. *Geophysical Research Letters*, *46*(14), 8261–8270. https://doi.org/10.1029/2019GL082513

Campos, M. C., Chiessi, C. M., Novello, V. F., Crivellari, S., Campos, J. L. P. S., Albuquerque, A. L. S., et al. (2022). South American precipitation dipole forced by interhemispheric temperature gradient. *Scientific Reports*, *12*(1), 10527. https://doi.org/10.1038/s41598-022-14495-1

Caves, J. K., Winnick, M. J., Graham, S. A., Sjostrom, D. J., Mulch, A., & Chamberlain, C. P. (2015). Role of the westerlies in Central Asia climate over the Cenozoic. *Earth and Planetary Science Letters*, *428*, 33–43. https://doi.org/10.1016/j.epsl.2015.07.023

Chamberlain, C. P., Winnick, M. J., Mix, H. T., Chamberlain, S. D., & Maher, K. (2014). The impact of neogene grassland expansion and aridification on the isotopic composition of continental precipitation. *Global Biogeochemical Cycles*, *28*(9), 992–1004. https://doi.org/10.1002/2014GB004822

Cheng, H., Sinha, A., Cruz, F. W., Wang, X., Edwards, R. L., D'Horta, F. M., et al. (2013). Climate change patterns in Amazonia and biodiversity. *Nature Communications*, *4*, 1–6. https://doi.org/10.1038/ncomms2415

Chiessi, C. M., Mulitza, S., Taniguchi, N. K., Prange, M., Campos, M. C., Häggi, C., et al. (2021). Mid to late Holocene contraction of the intertropical convergence zone over northeastern south America. *Paleoceanography and Paleoclimatology*, *36*(4), e2020PA003936. https://doi.org/10.1029/2020PA003936

Comas-Bru, L., Atsawawaranunt, K., & Harrison, S., & SISAL working group members. (2022). SISAL (speleothem isotopes Synthesis and AnaLysis working group) database version 2.0 [Dataset]. University of Reading. https://doi.org/10.17864/1947.256

Comas-Bru, L., Harrison, S. P., Werner, M., Rehfeld, K., Scroxton, N., Veiga-Pires, C., & SISAL working group members. (2019). Evaluating model outputs using integrated global speleothem records of climate change since the last glacial. *Climate of the Past*, *15*(4), 1557–1579. https://doi.org/10.5194/cp-15-1557-2019

Comas-Bru, L., Rehfeld, K., Roesch, C., Amirnezhad-Mozhdehi, S., Harrison, S. P., Atsawawaranunt, K., et al. (2020). SISALv2: A comprehensive speleothem isotope database with multiple age–depth models. *Earth System Science Data*, *12*(4), 2579–2606. https://doi.org/10.5194/essd-12-2579-2020

Cruz, F. W., Vuille, M., Burns, S. J., Wang, X., Cheng, H., Werner, M., et al. (2009). Orbitally driven east–west antiphasing of South American precipitation. *Nature Geoscience*, *2*(3), 210–214. https://doi.org/10.1038/ngeo444

Dee, S., Noone, D., Buenning, N., Emile-Geay, J., & Zhou, Y. (2015). SPEEDY-IER: A fast atmospheric GCM with water isotope physics. *Journal of Geophysical Research: Atmospheres*, *120*(1), 73–91. https://doi.org/10.1002/2014JD022194

De Oliveira, P. E., Barreto, A. M. F., & Suguio, K. (1999). Late Pleistocene/Holocene climatic and vegetational history of the Brazilian caatinga: The fossil dunes of the middle São Francisco River. *Palaeogeography, Palaeoclimatology, Palaeoecology*, *152*(3–4), 319–337. https://doi.org/10.1016/S0031-0182(99)00061-9

Deplazes, G., Lückge, A., Peterson, L. C., Timmermann, A., Hamann, Y., Hughen, K. A., et al. (2013). Links between tropical rainfall and North Atlantic climate during the last glacial period. *Nature Geoscience*, *6*(3), 213–217. https://doi.org/10.1038/ngeo1712

Ford, H. L., McChesney, C. L., Hertzberg, J. E., & McManus, J. F. (2018). A deep eastern equatorial Pacific thermocline during the Last Glacial Maximum. *Geophysical Research Letters*, *45*(21), 11806–11816. https://doi.org/10.1029/2018GL079710

Fornace, K. L., Whitney, B. S., Galy, V., Hughen, K. A., & Mayle, F. E. (2016). Late Quaternary environmental change in the interior South American tropics: New insight from leaf wax stable isotopes. *Earth and Planetary Science Letters*, *438*, 75–85. https://doi.org/10.1016/j.epsl.2016.01.007

Fritz, S. C., Baker, P. A., Lowenstein, T. K., Seltzer, G. O., Rigsby, C. A., Dwyer, G. S., et al. (2004). Hydrologic variation during the last 170,000 years in the southern hemisphere tropics of South America. *Quaternary Research*, *61*(01), 95–104. https://doi.org/10.1016/j.yqres.2003.08.007

Garreaud, R. D., Vuille, M., Compagnucci, R., & Marengo, J. (2009). Present-day South American climate. *Palaeogeography, Palaeoclimatology, Palaeoecology*, *281*(3–4), 180–195. https://doi.org/10.1016/j.palaeo.2007.10.032

Gat, J. R., & Matsui, E. (1991). Atmospheric water balance in the Amazon basin: An isotopic evapotranspiration model. *Journal of Geophysical Research*, *96*(D7), 13179. https://doi.org/10.1029/91JD00054

Grootes, P. M., Stuiver, M., Thompson, L. G., & Mosley-Thompson, E. (1989). Oxygen isotope changes in tropical ice, Quelccaya, Peru. *Journal of Geophysical Research*, *94*(D1), 1187. https://doi.org/10.1029/JD094iD01p01187

Häggi, C., Chiessi, C. M., Merkel, U., Mulitza, S., Prange, M., Schulz, M., & Schefuß, E. (2017). Response of the Amazon rainforest to late Pleistocene climate variability. *Earth and Planetary Science Letters*, *479*, 50–59. https://doi.org/10.1016/j.epsl.2017.09.013

Haug, G. H., Hughen, K. A., Sigman, D. M., Peterson, L. C., & Röhl, U. (2001). Southward migration of the intertropical convergence zone through the Holocene. *Science*, *293*(5533), 1304–1308. https://doi.org/10.1126/science.1059725

Hu, C., Henderson, G. M., Huang, J., Xie, S., Sun, Y., & Johnson, K. R. (2008). Quantification of Holocene Asian monsoon rainfall from spatially separated cave records. *Earth and Planetary Science Letters*, *266*(3–4), 221–232. https://doi.org/10.1016/j.epsl.2007.10.015

Huth, T. E., Passey, B. H., Cole, J. E., Lachniet, M. S., McGee, D., Denniston, R. F., et al. (2022). A framework for triple oxygen isotopes in speleothem paleoclimatology. *Geochimica et Cosmochimica Acta*, *319*, 191–219. https://doi.org/10.1016/j.gca.2021.11.002

Kanner, L. C., Burns, S. J., Cheng, H., & Edwards, R. L. (2012). High-latitude forcing of the South American summer monsoon during the last glacial. *Science*, *335*(6068), 570–573. https://doi.org/10.1126/science.1213397

Keys, P. W., van der Ent, R. J., Gordon, L. J., Hoff, H., Nikoli, R., & Savenije, H. H. G. (2012). Analyzing precipitationsheds to understand the vulnerability of rainfall dependent regions. *Biogeosciences*, *9*(2), 733–746. https://doi.org/10.5194/bg-9-733-2012

Konecky, B. L., Noone, D. C., & Cobb, K. M. (2019). The influence of competing hydroclimate processes on stable isotope ratios in tropical rainfall. *Geophysical Research Letters*, *46*(3), 1622–1633. https://doi.org/10.1029/2018GL080188

Koutavas, A., & Joanides, S. (2012). El Niño-Southern Oscillation extrema in the Holocene and last glacial maximum: ENSO extrema in the holocene and LGM. *Paleoceanography*, *27*(4), PA4208. https://doi.org/10.1029/2012PA002378

Kukla, T., Ahlström, A., Maezumi, S. Y., Chevalier, M., Lu, Z., Winnick, M. J., & Chamberlain, C. P. (2021). The resilience of Amazon tree cover to past and present drying. *Global and Planetary Change*, *202*, 103520. https://doi.org/10.1016/j.gloplacha.2021.103520

Kukla, T., Winnick, M. J., Laguë, M. M., & Xia, Z. (2022). tykukla/zonalprecippatterns-amazon: Zenodo release v1.2 (v1.2) [Dataset]. Zenodo. https://doi.org/10.5281/zenodo.7495709

Kukla, T., Winnick, M. J., Maher, K., Ibarra, D. E., & Chamberlain, C. P. (2019). The sensitivity of terrestrial δ^{18}O gradients to hydroclimate evolution. *Journal of Geophysical Research: Atmospheres*, *124*(2), 563–582. https://doi.org/10.1029/2018JD029571

Laguë, M. M., Bonan, G. B., & Swann, A. L. S. (2019). Separating the impact of individual land surface properties on the terrestrial surface energy budget in both the coupled and uncoupled land–atmosphere system. *Journal of Climate*, *32*(18), 20–5744. https://doi.org/10.1175/jcli-d-18-0812.1

Laguë, M. M., Swann, A. L. S., & Boos, W. R. (2021). Radiative feedbacks on land surface change and associated tropical precipitation shifts. *Journal of Climate*, *34*(16), 6651–6672. https://doi.org/10.1175/JCLI-D-20-0883.1

Lee, J.-E., Johnson, K., & Fung, I. (2009). Precipitation over South America during the Last Glacial Maximum: An analysis of the "amount effect" with a water isotope-enabled general circulation model. *Geophysical Research Letters*, *36*(19), L19701. https://doi.org/10.1029/2009GL039265

Li, W., Fu, R., & Dickinson, R. E. (2006). Rainfall and its seasonality over the Amazon in the 21st century as assessed by the coupled models for the IPCC AR4. *Journal of Geophysical Research*, *111*(D2), D02111. https://doi.org/10.1029/2005JD006355

Liu, X., & Battisti, D. S. (2015). The influence of orbital forcing of tropical insolation on the climate and isotopic composition of precipitation in South America. *Journal of Climate*, *28*(12), 4841–4862. https://doi.org/10.1175/JCLI-D-14-00639.1

Lu, Z., Zhang, Q., Miller, P. A., Zhang, Q., Berntell, E., & Smith, B. (2021). Impacts of large-scale Sahara solar farms on global climate and vegetation cover. *Geophysical Research Letters*, *48*(2), e2020GL090789. https://doi.org/10.1029/2020GL090789

Martin, L., Bertaux, J., Corrège, T., Ledru, M.-P., Mourguiart, P., Sifeddine, A., et al. (1997). Astronomical forcing of contrasting rainfall changes in tropical South America between 12,400 and 8800 cal yr B.P. *Quaternary Research*, *47*(1), 117–122. https://doi.org/10.1006/qres.1996.1866

Mason, C. C., Romans, B. W., Stockli, D. F., Mapes, R. W., & Fildani, A. (2019). Detrital zircons reveal sea-level and hydroclimate controls on Amazon River to deep-sea fan sediment transfer. *Geology*, *47*(6), 563–567. https://doi.org/10.1130/G45852.1

McGee, D., de Menocal, P., Winckler, G., Stuut, J., & Bradtmiller, L. (2013). The magnitude, timing and abruptness of changes in North African dust deposition over the last 20,000yr. *Earth and Planetary Science Letters*, *371–372*, 163–176. https://doi.org/10.1016/j.epsl.2013.03.054

McIntyre, A., & Molfino, B. (1996). Forcing of Atlantic equatorial and subpolar millennial cycles by precession. *Science*, *274*(5294), 1867–1870. https://doi.org/10.1126/science.274.5294.1867

Mosblech, N. A. S., Bush, M. B., Gosling, W. D., Hodell, D., Thomas, L., van Calsteren, P., et al. (2012). North Atlantic forcing of Amazonian precipitation during the last ice age. *Nature Geoscience*, *5*(11), 817–820. https://doi.org/10.1038/ngeo1588

Mulitza, S., Chiessi, C. M., Schefuß, E., Lippold, J., Wichmann, D., Antz, B., et al. (2017). Synchronous and proportional deglacial changes in Atlantic meridional overturning and northeast Brazilian precipitation: AMOC and precipitation over NE Brazil. *Paleoceanography*, *32*(6), 622–633. https://doi.org/10.1002/2017PA003084

Nace, T. E., Baker, P. A., Dwyer, G. S., Silva, C. G., Rigsby, C. A., Burns, S. J., et al. (2014). The role of North Brazil Current transport in the paleoclimate of the Brazilian Nordeste margin and paleoceanography of the western tropical Atlantic during the late Quaternary. *Palaeogeography, Palaeoclimatology, Palaeoecology*, *415*, 3–13. https://doi.org/10.1016/j.palaeo.2014.05.030

Nogués-Paegle, J., & Mo, K. C. (1997). Alternating wet and dry conditions over South America during summer. *Monthly Weather Review*, *125*(2), 279–291. https://doi.org/10.1175/1520-0493(1997)125⟨0279:AWADCO⟩2.0.CO;2

Novello, V. F., Cruz, F. W., Moquet, J. S., Vuille, M., de Paula, M. S., Nunes, D., et al. (2018). Two millennia of South Atlantic Convergence Zone variability reconstructed from isotopic proxies. *Geophysical Research Letters*, *45*(10), 5045–5051. https://doi.org/10.1029/2017GL076838

Novello, V. F., Cruz, F. W., Vuille, M., Stríkis, N. M., Edwards, R. L., Cheng, H., et al. (2017). A high-resolution history of the South American monsoon from Last Glacial Maximum to the Holocene. *Scientific Reports*, *7*(1), 44267. https://doi.org/10.1038/srep44267

Pattnayak, K., Tindall, J., Brienen, R., Barichivich, J., & Gloor, E. (2019). Can we detect changes in Amazon forest structure using measurements of the isotopic composition of precipitation? *Geophysical Research Letters*, *46*(24), 14807–14816. https://doi.org/10.1029/2019GL084749

Prado, L. F., Wainer, I., & Chiessi, C. M. (2013). Mid-Holocene PMIP3/CMIP5 model results: Intercomparison for the South American monsoon system. *The Holocene*, *23*(12), 1915–1920. https://doi.org/10.1177/0959683613505336

Prentice, I. C., Harrison, S. P., & Bartlein, P. J. (2011). Global vegetation and terrestrial carbon cycle changes after the last ice age. *New Phytologist*, *189*(4), 988–998. https://doi.org/10.1111/j.1469-8137.2010.03620.x

Reis, L. S., Guimarães, J. T. F., Souza-Filho, P. W. M., Sahoo, P. K., de Figueiredo, M. M. J. C., de Souza, E. B., & Giannini, T. C. (2017). Environmental and vegetation changes in southeastern Amazonia during the late Pleistocene and Holocene. *Quaternary International*, *449*, 83–105. https://doi.org/10.1016/j.quaint.2017.04.031

Ribas, C. C., Fritz, S. C., & Baker, P. A. (2022). The challenges and potential of geogenomics for biogeography and conservation in Amazonia. *Journal of Biogeography*, *49*(10), 1839–1847. https://doi.org/10.1111/jbi.14452

Salati, E., Dall'Olio, A., Matsui, E., & Gat, J. R. (1979). Recycling of water in the Amazon Basin: An isotopic study. *Water Resources Research*, *15*(5), 1250–1258. https://doi.org/10.1029/WR015i005p01250

Scheff, J., & Frierson, D. M. W. (2014). Scaling potential evapotranspiration with greenhouse warming. *Journal of Climate*, *27*(4), 1539–1558. https://doi.org/10.1175/JCLI-D-13-00233.1

Shanahan, T. M., McKay, N. P., Hughen, K. A., Overpeck, J. T., Otto-Bliesner, B., Heil, C. W., et al. (2015). The time-transgressive termination of the African Humid Period. *Nature Geoscience*, *8*(2), 140–144. https://doi.org/10.1038/ngeo2329

Sherwood, S. C., Ingram, W., Tsushima, Y., Satoh, M., Roberts, M., Vidale, P. L., & O'Gorman, P. A. (2010). Relative humidity changes in a warmer climate. *Journal of Geophysical Research*, *115*(D9), D09104. https://doi.org/10.1029/2009JD012585

Shimizu, M. H., Sampaio, G., Venancio, I. M., & Maksic, J. (2020). Seasonal changes of the South American monsoon system during the Mid-Holocene in the CMIP5 simulations. *Climate Dynamics*, *54*(5–6), 2697–2712. https://doi.org/10.1007/s00382-020-05137-1

Siler, N., Roe, G. H., Armour, K. C., & Feldl, N. (2019). Revisiting the surface-energy-flux perspective on the sensitivity of global precipitation to climate change. *Climate Dynamics*, *52*(7–8), 3983–3995. https://doi.org/10.1007/s00382-018-4359-0

Skonieczny, C., McGee, D., Winckler, G., Bory, A., Bradtmiller, L. I., Kinsley, C. W., et al. (2019). Monsoon-driven Saharan dust variability over the past 240,000 years. *Science Advances*, *5*(1), eaav1887. https://doi.org/10.1126/sciadv.aav1887

Staal, A., Tuinenburg, O. A., Bosmans, J. H. C., Holmgren, M., van Nes, E. H., Scheffer, M., et al. (2018). Forest-rainfall cascades buffer against drought across the Amazon. *Nature Climate Change*, *8*(6), 539–543. https://doi.org/10.1038/s41558-018-0177-y

Tapia, P. M., Fritz, S. C., Baker, P. A., Seltzer, G. O., & Dunbar, R. B. (2003). A Late Quaternary diatom record of tropical climatic history from Lake Titicaca (Peru and Bolivia). *Palaeogeography, Palaeoclimatology, Palaeoecology*, *194*(1–3), 139–164. https://doi.org/10.1016/S0031-0182(03)00275-X

Tigchelaar, M., & Timmermann, A. (2016). Mechanisms rectifying the annual mean response of tropical Atlantic rainfall to precessional forcing. *Climate Dynamics*, *47*(1–2), 271–293. https://doi.org/10.1007/s00382-015-2835-3

van Breukelen, M., Vonhof, H., Hellstrom, J., Wester, W., & Kroon, D. (2008). Fossil dripwater in stalagmites reveals Holocene temperature and rainfall variation in Amazonia. *Earth and Planetary Science Letters*, *275*(1–2), 54–60. https://doi.org/10.1016/j.epsl.2008.07.060

van der Ent, R. J. (2016). WAM-2 layers Python.

van der Ent, R. J., & Savenije, H. H. G. (2013). Oceanic sources of continental precipitation and the correlation with sea surface temperature: Precipitation and Correlation with SST. *Water Resources Research*, *49*(7), 3993–4004. https://doi.org/10.1002/wrcr.20296

van der Ent, R. J., Wang-Erlandsson, L., Keys, P. W., & Savenije, H. H. G. (2014). Contrasting roles of interception and transpiration in the hydrological cycle – Part 2: Moisture recycling. *Earth System Dynamics*, *5*(2), 471–489. https://doi.org/10.5194/esd-5-471-2014

Venancio, I. M., Mulitza, S., Govin, A., Santos, T. P., Lessa, D. O., Albuquerque, A. L. S., et al. (2018). Millennial- to orbital-scale responses of western equatorial Atlantic thermocline depth to changes in the trade wind system since the last interglacial. *Paleoceanography and Paleoclimatology*, *33*(12), 1490–1507. https://doi.org/10.1029/2018PA003437

Vimeux, F., Gallaire, R., Bony, S., Hoffmann, G., & Chiang, J. (2005). What are the climate controls on δD in precipitation in the Zongo valley (Bolivia)? Implications for the Illimani ice core interpretation. *Earth and Planetary Science Letters*, *240*(2), 205–220. https://doi.org/10.1016/j.epsl.2005.09.031

Vuille, M., Bradley, R. S., Werner, M., Healy, R., & Keimig, F. (2003). Modeling δ18O in precipitation over the tropical Americas: 1. Interannual variability and climatic controls. *Journal of Geophysical Research*, *108*(D6), 4174. https://doi.org/10.1029/2001JD002038

Vuille, M., & Werner, M. (2005). Stable isotopes in precipitation recording South American summer monsoon and ENSO variability: Observations and model results. *Climate Dynamics*, *25*(4), 401–413. https://doi.org/10.1007/s00382-005-0049-9

Wang, X., Auler, A. S., Edwards, R. L., Cheng, H., Cristalli, P. S., Smart, P. L., et al. (2004). Wet periods in northeastern Brazil over the past 210 kyr linked to distant climate anomalies. *Nature*, *432*(7018), 740–743. https://doi.org/10.1038/nature03067

Wang, X., Edwards, R. L., Auler, A. S., Cheng, H., Kong, X., Wang, Y., et al. (2017). Hydroclimate changes across the Amazon lowlands over the past 45,000 years. *Nature*, *541*(7636), 204–207. https://doi.org/10.1038/nature20787

Ward, B. M., Wong, C. I., Novello, V. F., McGee, D., Santos, R. V., Silva, L. C., et al. (2019). Reconstruction of Holocene coupling between the South American Monsoon System and local moisture variability from speleothem δ18O and 87Sr/86Sr records. *Quaternary Science Reviews*, *210*, 51–63. https://doi.org/10.1016/j.quascirev.2019.02.019

Whitney, B. S., Mayle, F. E., Punyasena, S. W., Fitzpatrick, K. A., Burn, M. J., Guillen, R., et al. (2011). A 45 kyr palaeoclimate record from the lowland interior of tropical South America. *Palaeogeography, Palaeoclimatology, Palaeoecology*, *307*(1–4), 177–192. https://doi.org/10.1016/j.palaeo.2011.05.012

Winnick, M. J., Chamberlain, C. P., Caves, J. K., & Welker, J. M. (2014). Quantifying the isotopic' continental effect. *Earth and Planetary Science Letters*, *406*, 123–133. https://doi.org/10.1016/j.epsl.2014.09.005

Worden, J., Noone, D., Bowman, K., & Tropospheric Emission Spectrometer science team and data. (2007). Importance of rain evaporation and continental convection in the tropical water cycle. *Nature*, *445*(7127), 528–532. https://doi.org/10.1038/nature05508

Wortham, B. E., Wong, C. I., Silva, L. C., McGee, D., Montañez, I. P., Troy Rasbury, E., et al. (2017). Assessing response of local moisture conditions in central Brazil to variability in regional monsoon intensity using speleothem 87Sr/86Sr values. *Earth and Planetary Science Letters*, *463*, 310–322. https://doi.org/10.1016/j.epsl.2017.01.034

Wu, H., Guiot, J., Brewer, S., & Guo, Z. (2007). Climatic changes in Eurasia and Africa at the last glacial maximum and mid-Holocene: Reconstruction from pollen data using inverse vegetation modelling. *Climate Dynamics*, *29*(2–3), 211–229. https://doi.org/10.1007/s00382-007-0231-3

Zemp, D. C., Schleussner, C.-F., Barbosa, H. M. J., Hirota, M., Montade, V., Sampaio, G., et al. (2017). Self-amplified Amazon forest loss due to vegetation-atmosphere feedbacks. *Nature Communications*, *8*(1), 14681. https://doi.org/10.1038/ncomms14681

Zular, A., Sawakuchi, A. O., Chiessi, C. M., d'Horta, F. M., Cruz, F. W., Demattê, J. A. M., et al. (2019). The role of abrupt climate change in the formation of an open vegetation enclave in northern Amazonia during the Late Quaternary. *Global and Planetary Change*, *172*, 140–149. https://doi.org/10.1016/j.gloplacha.2018.09.006